Synthesis and Characterization of Sulphur Doped SnSb for Photovoltaic Applications

By

Muhammad Raies Abdullah

(266-FBAS/MSPHY/S14)

Supervisor:

Dr. Waqar Adil Syed

Associate Professor, Department of Physics, FBAS, IIUI

DEPARTMENT OF PHYSICS

FACULTY OF BASIC AND APPLIED SCIENCES

INTERNATIONAL ISLAMIC UNIVERSITY, ISLAMABAD

(2016)

Thin film devices
Nanotechnology
X-Ray diffraction
Chemical vapor deposition

INTERNATIONAL ISLAMIC UNIVERSITY, ISLAMABAD

FACULTY OF BASIC AND APPLIED SCIENCES

DEPARTMENT OF PHYSICS

(2017)

Synthesis and Characterization of Sulphur Doped SnSb for Photovoltaic Applications

By

Muhammad Raies Abdullah

(266-FBAS/MSPHY/S14)

A Thesis Submitted to

Department of Physics, Faculty of Basic and Applied Sciences, International Islamic University, Islamabad (IIUI) for the Award of the

Degree of

MS PHYSICS

Chairman department of Physics

International Islamic University, Islamabad

CHAIRMAN
DEPT. OF PHYSICS
International Islamic University
Islamabad

Dean FBAS

International Islamic University, Islamabad

Final approval

It is certified that work presented in this thesis entitled "**Synthesis and Characterization of Sulphur Doped SnSb for Photovoltaic Applications**" by **Muhammad Raies Abdullah**, Registration No. 266-FBAS/MSPHY/F10 fulfills the requirement for the award of degree from of MS Physics from the Department of Physics, International Islamic University, Islamabad, Pakistan.

Viva voce Committee

Chairman _____

(Department of Physics)

Supervisor _____

External Examiner _____

Internal Examiner _____

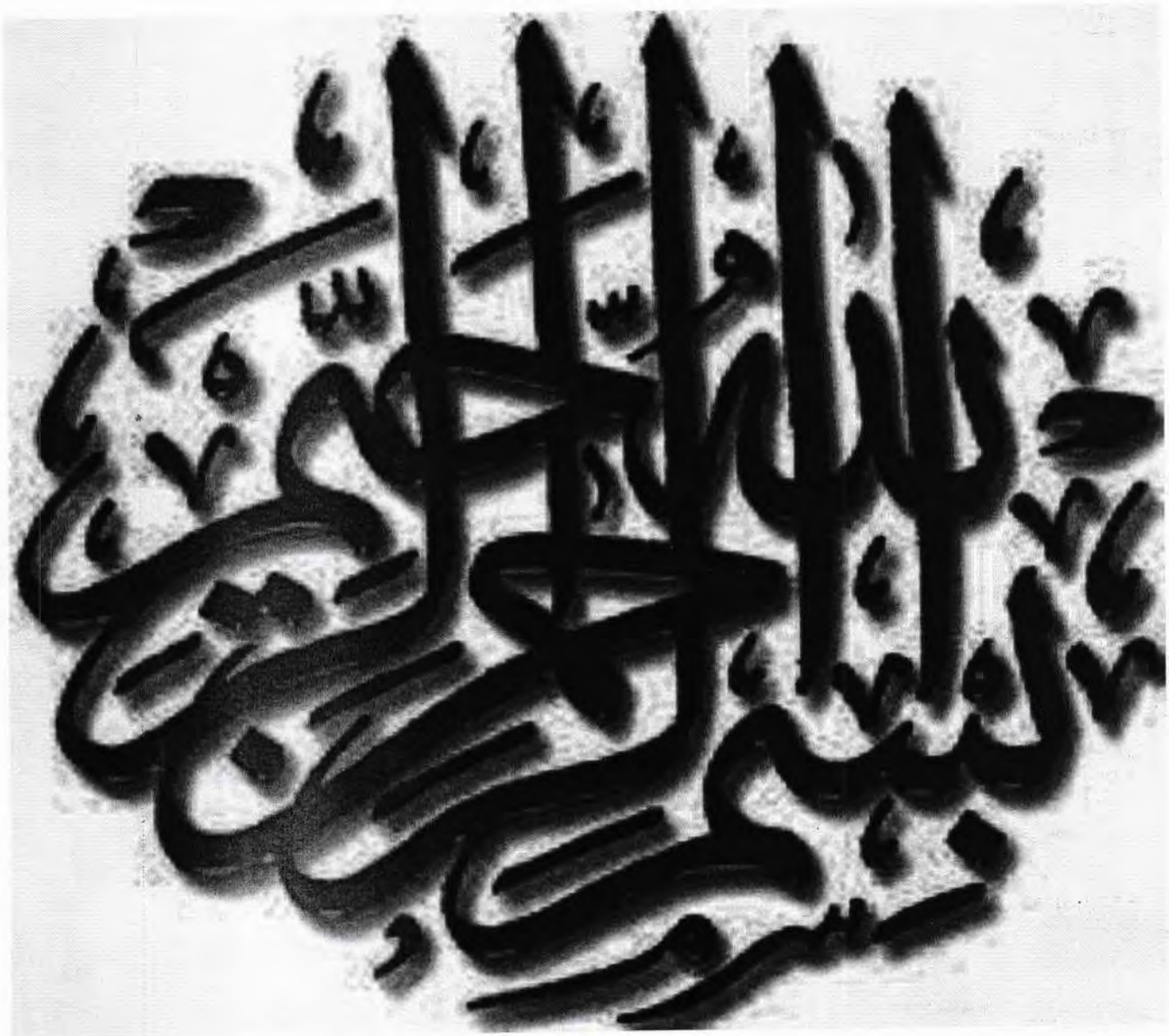

Thesis submitted to

Department of Physics

International Islamic University Islamabad

As a partial fulfillment for the award of the degree of

MS Physics

Declaration

I hereby declare that this thesis work, neither as a whole nor a part of it has been copied out from any source. Further, work presented in this dissertation has not been submitted in support of any application for any other degree or qualification to any other university or institute and considerable under the plagiarism rules of Higher Education Commission (HEC), Pakistan.

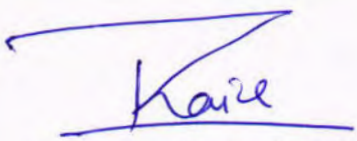

Muhammad Raies Abdullah

(266-FBAS/MSPHY/S14)

Certificate

It is certified that work contained in this thesis is carried out by Muhammad Raies Abdullah under my supervision at the Department of Physics, International Islamic University,Islamabad, Pakistan.

Supervisor:

Dr. Waqar Adil Syed

Associate Professor

Department of Physics, FBAS, IIUI

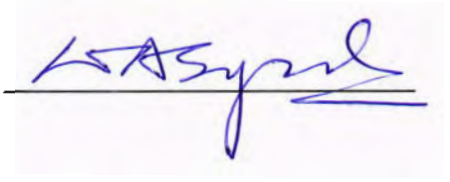

DEDICATIONS

This work is dedicated to my Parents who remembered me in their prayers, under their shadow of love; perhaps it could be impossible to attain this target.

I also dedicate this work and give special thanks to my Lab mates and friends who have supported me throughout the process. I will always appreciate all they have done for me.

.

ACKNOWLEDGEMENT

I have really no words to express the deepest sense of gratitude to Almighty **ALLAH** the most merciful and compassionate, the Creator of the universe, **WHO** giving me the strength and perseverance for completing the research. I offer my humblest and sincerest words of thanks to the **Holy Prophet** (P.B.U.H) who is always a torch of guidance and knowledge for humanity.

It is a matter of great pleasure and honor for me to express my deep sense of devotion and deepest gratitude to **Dr. Waqar Adil Syed**, Associate Professor, Department of Physics, International Islamic University, Islamabad as supervisor.

Finally, I acknowledge the help, the encouragement, endless love, support and prayers of my family and my colleagues specially counter strike team (Lab Mates) which have always been a source of inspiration and guidance for me all the way.

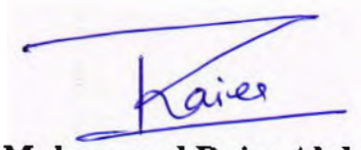

Muhammad Raies Abdullah

ABSTRACT

Tin antimony sulfide thin films have been deposited on glass substrate at room temperature by thermal evaporation method. The doping was done by two source method with the purpose to investigate its consequences on structural, electrical and optical properties of Sn-doped Sb_2S_3 thin films. XRD studies revealed that both the as deposited and annealed films exist in $Sn_2Sb_2S_5$ phase. The accurate information about composition and concentration depth of the as-deposited and annealed $Sn_2Sb_2S_5$ films were recorded by Rutherford backscattering spectroscopy (RBS) technique. Photoconductivity response of these films was also fine and enhanced with the increasing concentration of tin sulfide. High transmittance was found below 750 nm which decreased with annealing temperature. The band gap calculated by ellipsometry technique was in the range 1.68-2.31 eV. Thickness of the film was observed as 240 nm and the films possess n-type conductivity.

Table of Contents

CHAPTER 1 ..... **1**

1 INTRODUCTION **1**

1.1 Introduction 1

1.2 Thin Film Technology 1

1.2.1 Importance of Thin Films 2

1.3 Introduction to Materials 2

1.3.1 Tin Antimony Sulfide 3

1.3.2 Tin (Sn) 4

1.3.3 Antimony (Sb) 4

1.4 Tin Sulfide (SnS) 5

1.5 Antimony Sulfide 6

1.6 Thesis Motivation and Objective 7

1.7 References 8

CHAPTER 2 ..... **11**

2 LITERATURE SURVEY **11**

2.1 References 15

CHAPTER 3 ..... **17**

3 EXPERIMENTAL SETUP AND WORK **17**

3.1 Thin Film Deposition 17

3.2 Thin Film Deposition Techniques 18

3.2.1 Chemical Vapor Deposition 19

3.2.2 Deposition of Physical Vapor Process 19

3.2.3 Close spaced sublimation (CSS) 20

3.3 Two Source Sublimation Technique 20

3.4 Deposition of SnS on thin Sb_2S_3 films using sputtering method 22

3.4.1 Deposition parameters 22

3.5 Characterization Techniques Used for Tin Antimony Sulfide Thin Films 23

3.5.1 Rutherford Backscattering Spectrometry (RBS) 23

3.5.2 Proton Induced X-Ray Emission (PIXE) 25
3.5.3 X-Ray Diffraction (XRD) 26
3.5.4 Spectroscopic Ellipsometery (SE) 28
3.5.5 Scanning Electron Microscopy 33
3.5.6 Hall measurement 35
3.6 References 37
CHAPTER 4 ..... **39**
4 Result and Discussions **39**
4.1 Structural Analysis: 39
4.2 Surface Morphology 42
4.2.1 SEM (Scanning Electron Microscope) 42
4.3 Elemental Analysis 44
4.3.1 RBS (Rutherford backscattering spectroscopy) 44
4.3.2 Proton Induced X-ray Emission (PIXE) 45
4.4 Optical Analysis 45
4.4.1 Reflectance 50
4.4.2 Extinction coefficient. 50
4.4.3 Refractive index 51
4.5 Electrical Analysis 52
4.6 Conclusions 54

List of figures

Figure 1. 1: Structure of different compounds 3

Figure 1. 2: Structure of Tin Sulfide 5

Figure 3. 1: Two Source sublimation technique schematic diagram. 21

Figure 3. 2: Experimental set up of close spaced sublimation Chamber 22

Figure 3. 3: Schematic of RBS instrument 24

Figure 3. 4: A 5UDH-2 Pelletron Tandem Accelerator at NCP, Islamabad 25

Figure 3. 5: Schematic diagram of PIXE 26

Figure 3. 6: Bragg's diffraction 27

Figure 3. 7: (XRD) X-ray diffraction machine 28

Figure 3. 8: Schematic diagram of spectroscopic ellipsometry technique 30

Figure 3. 9: Spectroscopic ellipsometry system at IIUI 31

Figure 3. 10: Schematic diagram of SEM 34

Figure 3. 11: Hall schematic diagram 36

Figure 4. 2: 3-D pattern of XRD 41

Figure 4. 3: SEM image of S1 (tin antimony sulfide) 42

Figure 4. 4: SEM images of S2 (tin antimony sulfide) 42

Figure 4. 5: SEM image S3(tin antimony sulfide) 43

Figure 4. 6: SEM images of S4 & S5 (tin antimony sulfide) 43

Figure 4. 7: Rutherford backscattering spectra of all samples 44

Figure 4. 8: Absorption coefficient of prepared thin films by Elipsometry 46

Figure 4. 9: Plotting band gap of prepared thin film for S1 47

Figure 4. 10: Plotting band gap of prepared thin film for S2 48

Figure 4. 11: Plotting band gap of prepared thin film for S3 48

Figure 4. 12: Plotting band gap of prepared thin film for S4 49

Figure 4. 13: Plotting band gap of prepared thin film for S5 49

Figure 4. 14: Reflectance of tin antimony sulfide by ellipsometry 50

Figure 4. 15 : Extinction coefficient for $Sn_2Sb_2S_5$ 51

Figure 4. 16: Refractive index graphs 51

Figure 4. 17: Graph for I-V 53

List of tables

Table 1. 1: Some physical properties of Tin 4

Table 1. 2 : Physical properties of Antimony..... 5

Table 4. 1: Structural data obtained from XRD measurement..... 41

Table 4. 2: RBS Thickness and elemental composition by PIXE..... 45

Table 4. 3: Thickness of thin films by Ellipsometry..... 46

Table 4. 4 : Table for Hall Measurement..... 52

CHAPTER 1

1 INTRODUCTION

1.1 Introduction

This project has been accomplished with an aim to study the physical properties of Tin Antimony sulfide films deposited by two source method. The concentration of tin has been varied and effect of post annealing temperature is studied in detail. These changed properties of thin films have been investigated by concentration depth profiles determined by Rutherford backscattering spectroscopy (RBS) technique. This method has been used to determine the composition, film thickness, stoichiometry and concentration depth profiles in semiconductors and metal thin films. Various applications of the Rutherford backscattering spectroscopy have been discussed. Extensive discussion based upon electronic interaction where scientists involved in this phenomenon can exchange and discuss ideas, information and new scientific concepts. Several other structural and optical properties of the prepared nano-crystalline Tin Antimony Sulfide thin films have also been studied.

1.2 Thin Film Technology

Thin films have very thin layer with a particular high surface-to-volume ratio. These are the layers of materials varying from fractions of a nanometer to more than a few microns in thickness. Films are considered as thin, if we can create the surface properties with the purpose of distinctly different properties from the bulk. In thin films, the forces which are acting on the surface atoms are completely different from those of the bulk. The reliability of thin films is subjected to the quality of its adhesion with the substrate, any residual or intrinsic stresses after the deposition, or the occurrence of surface defects or impurities. A film that peels off when the device is subjected to thermal or mechanical stresses can results in device failure. This adhesion depends primarily on the cleanliness of the substrate surface. A very smooth or rough substrate roughness also affects thin film adhesion.

There are always some intrinsic stresses while manufacturing the thin films, regardless of the deposition process. These stresses can either be compressive or tensile and can extend to adhesion tribulations, cracking and corrosion. Therefore, optimum deposition conditions are critical to minimize intrinsic stresses in the films [1]. Microelectronics is still one of the important fields in which thin film technology is being used. However, there are other rising and expanding applications in areas like magnetic and optical devices, shielding and nano-materials coatings [2]. Previously thin films have been engaged in making electronic devices and optical coatings etc. Now this substantial technology is being developed in the twenty-first century for the development of a new material such as nano-materials. The processing of thin films is also an energy saver process for the production of the devices [3].

1.2.1 Importance of Thin Films

Thin-film technologies are also being developed as a means of substantially reducing the cost of solar cells. Some applications require properties which occupy different features at the surface than those of the bulk, for example the operation of ICs depends on the electrical charges and the interface between dissimilar materials with diverse electronic properties. The desired properties of a composite material can be attained by producing it as bulk material and then coating a thin film on its surface. In the fabrication of lasers, geometrical and structural requirements are obtained by sandwiching different semiconductors in the form of films. Thin films also provide suitable coatings to enhance the effectiveness and extend the lifetime of the high temperature materials.

There are other various appliances where the exclusivity of thin films is important for the observed performance. Examples include: giant-magneto resistance films, thin film superconductors, super-lattice films and hetero structure lasers, etc [4, 5]. Micro-electromechanical systems (MEMS) are devised to operate as sensors and actuators [6]. Thin film deposition systems are merely accessible technique for coating of lenses and mirrors, also optical integrated circuits and micro-mechanical device manufacturing needs this particular technology for their implementation [7].

1.3 Introduction to Materials

Sb_2S_3 is member of V-VI layered semiconductor family. In last decades a lot of work have been done for the physical and chemical properties of chalcogenides films due to their wider range of applications in optoelectronic devices. In the range of available chalcogenides, pure and doped

Sb_2S_3 thin films are used in many important phenomenon like thermoelectric cooling technologies, solar energy conversion and because of photoconductive type target of TV screen. This is because of its high absorption coefficient (10^4 cm^{-1}) and having energy band gap [5-6] range 1.78 - 2.5eV [13-20]. It is widely used in optoelectronics, solar cells and solid state devices. As its energy gap for optical properties near about 1.3eV almost equivalent to that of Si. Tin antimony sulfide semiconductor would be of especial concern for photo-voltaic applications. Many techniques of deposition could be applied for SnS and Sb_2S_3 deposition e.g., chemical bath deposition, chemical vapor deposition, electro-deposition, electron beam, spray pyrolysis etc.

1.3.1 Tin Antimony Sulfide

Tin Antimony Sulfide is a chemical compound of III-V group of periodic table. The color of SnSbS is greyish-black and it is also direct band gap compound binary semiconductor. The value of band gap is almost 1.4eV to 3.4eV. SnSbS occurs naturally in the form of cubic zinc blende structure. Density is 5.27 g/cm^3, Molar mass of is 144.35g/mol, Melting point is 600 °C while its Refractive index is 2.67 on 550nm. Generally Metal-doped oxides of Tin are n-type semiconducting materials with richly electrical conductivity and well stability.

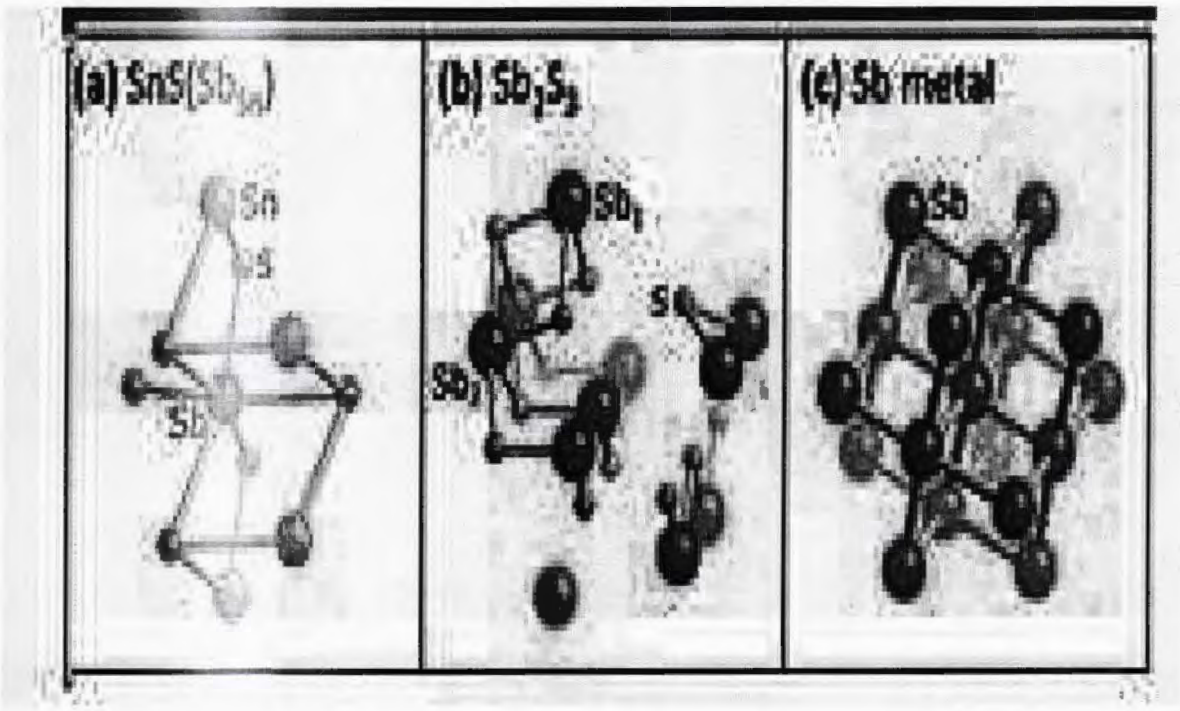

Figure 1. 1: Structure of different compounds

1.3.2 Tin (Sn)

Tin (**Sn**) is a element with atomic number 50 and electronic configuration given by [Kr] $4d^{10}$ $5s^2$ $5p^2$. Pure Sn has silvery lustrous grey color and is slightly soft and flexible. It is a metal with unbelievably high electrical and thermal conductivity. Tin becomes a superconductor below 3.72K. Also Tin was the first superconductors to be studied.

In oxygen solution Tin acts as a catalyst and helps quicken chemical reaction. This metal rejects erosion from purified, soft tap and sea water, but could defect by alkalis, acids, and by salt of acids. Sn have the greatest number of stable isotopes which is 10 (ten) along with 18 additional unstable isotopes are known.

Table 1. 1: Some physical properties of Tin

Electro-negativity	1.96
Melting point	231.9°C
Density	7.26 $g \cdot cm^{-3}$
current resistivity	16.78 $n\Omega \cdot m$
Structure of crystal	Tetragonal
Atomic radius	1247.8pm
Boiling point	2602°C
Hardness Mohs	1.5

1.3.3 Antimony (Sb)

Antimony (Sb) is a chemical element having atomic number 51 and electronic configuration is [Kr] $4d^{10}$ $5s^2$ $5p^3$. Pure Sb has silvery lustrous grey color. Antimony in its pure form is a brittle, silvery white, fusible, crystalline solid that indicates poor electrical and heat conductivity properties and evaporates at low temperatures. Antimony and some of its alloys are unusual in that they expand on cooling. The metalloid, antimony corresponds a metal in its visual aspect and physical properties, but does not chemically react as a metal.

Table 1. 2 : Physical properties of Antimony

Electro-negativity	2.05
Melting point	630.63°C
Density	6.69 $g \cdot cm^{-3}$
current resistivity	16.78 nΩ·m
Structure of crystal	Tetragonal
Atomic radius	1247.8pm
Boiling point	1587°C
Hardness Mohs	3.0

1.4 Tin Sulfide (SnS)

Tin sulfide is presently a leading compound for absorbing layers in next generation thin film solar cells. Presently, both Cadmium Telluride and Copper Indium Gallium Sulfide (CIGS) are used as p-type absorber layers, but they are developed from toxic, scarce constituents [24].Tin sulfide, by contrast, is formed from earth abundant elements, cheap and is nontoxic.

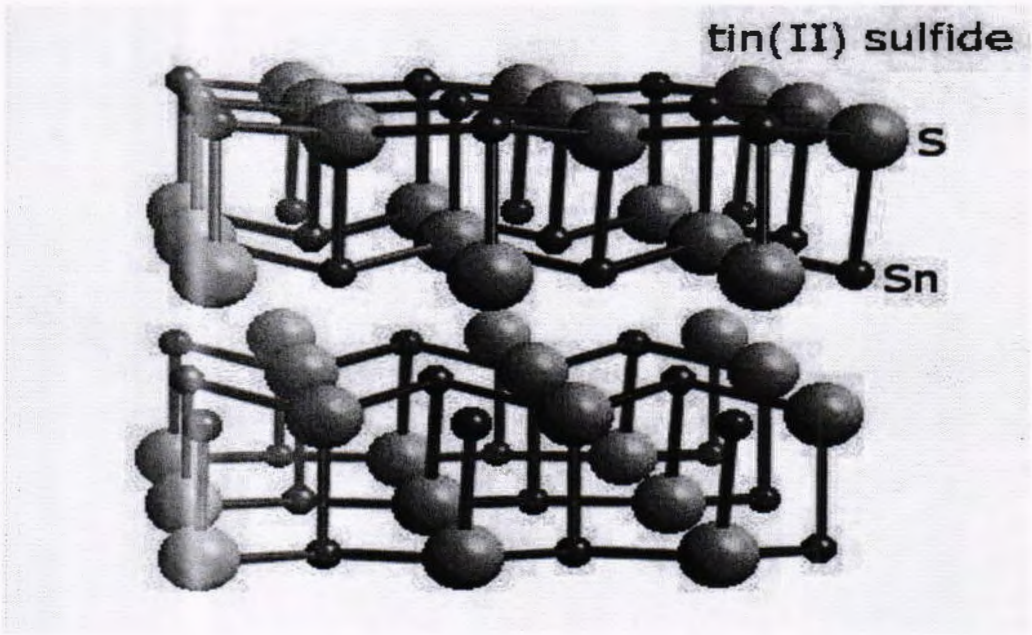

Figure 1. 2: Structure of Tin Sulfide

The structure of tin sulfide is shown in figure 1.3.This material also has a high optical absorption coefficient, p-type conductivity, and a midrange direct band gap of 1.3-1.4 eV, required electronic properties for this type of absorbing layer.[25] In fact, the energy conversion efficiency of tin sulfide is projected to be 32%, comparable to crystalline silicon.[26] Finally, Tin sulfide is stable in both alkaline and acidic conditions.[27] All previously mentioned characteristics propose tin sulfide as an optimal material for solar cells.

1.5 Antimony Sulfide

Good quality antimony sulfide thin films were prepared from a chemical bath containing $SbCl_3$ and $Na_2S_2O_3$ at room temperature. Upon heating in nitrogen, these films transformed into polycrystalline with stibnite structure. When the as-deposited Sb_2S_3 films were heated in air, initially they converted into polycrystalline stibnite phase which in turn transformed into Sb_2O_3 crystallites of Senarmontite phase during further heating. The values of optical band gap energy were evaluated as 2.57 and 1.73 eV for the as-deposited film and the film annealed in nitrogen respectively. [28]

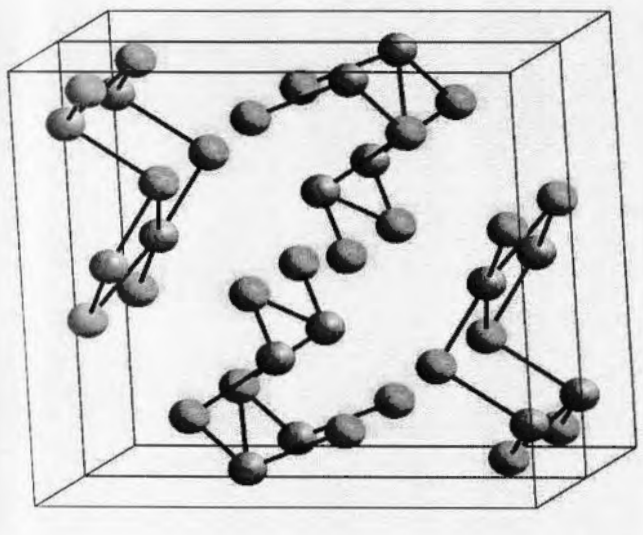

Figure 1.3: Structure of Antimony Sulfide

The crystal structure of Sb_2S_3 shown in figure 1.3. From the spectral dependences of absorption, the bandgap width was determined for the Sb_2Se_3 and Sb_2S_3 films are 1.66eV and 2.12 eV, respectively. The temperature dependences of the specific resistance had the activation nature, and

the obtained activation energies are evidence of stabilization of the Fermi level near the middle of the band gap.[29]

1.6 Thesis Motivation and Objective

The motivation regarding to my work is totally based on experimental work related to the compositional, structural and optical characteristics of SbS thin films with different Sn concentration. A number of researchers carried out enormous research work on SbS to examine the effects Sn of doping on different properties (structural, optical and electrical) by means of various synthesis and characterization techniques.

The core purpose of this research work is to study compositional, structural and optical properties in SbS thin films enriched with Sn. Tin creates acceptors levels which can be used in the optical processing. Cu have 0.68eV energy band gap range but use in variety of optical telecommunications [24]. Here we have motive that up to which extent Sulphur concentration affects crystal lattice, optical properties and crystalline quality of host material. Due to compositional and crystal changes whether we observe amorphous or semi crystalline character. Finally by process of subsequent post annealing after the deposition of films, how much we recover lattice damages/disorder in order to improve surface, structure and crystalline quality of the deposited thin films. For this reason my concentration throughout this dissertation is obviously on investigation of compositional, optical and structural properties of Sulphur or tin enriched Sn_xSbS_{1-x} thin films.

1.7 References

1. www.Siliconfareast.com/Thin_films_Semiconductor_manufacturing.
2. K. S Sree Harsha. Principls of physical vapor deposition. Elsevier (2006).
3. K. Wasa, M. Kitabatake, H. Adachi. Thin film material technology, sputtering of compound materials. Springer. William Andrew (2004).
4. K. S. Sree Harsha. Principles of Vapor Deposition of Thin Films (2006).
5. Kiyotaka Wasa. Thin film technology as a materials engineering. Revista Brasileira de Aplicacoes de Vacuo. **20** (2001).
6. S. Trolier-Mckinstry, P. Muralt. Thin Film Piezoelectrics for MEMS. Journal of Electroceramics **12** (2004) 7-17.
7. Christopher B Ebert, Loren A Eyres, Martin M Fejer, James S Harris Jr.. MBE growth of antiphase GaAs films using GaAs/Ge/GaAs heteroepitaxy, Journal of Crystal Growth **201–202** (1999) 187–193.
8. Torsten Rieger, Sonja Heiderich, Steffi Lenk, Mihail Ion Lepsa, Detlev Grützmacher, Ga-assisted MBE growth of GaAs nanowires using thin HSQ layer. Journal of Crystal Growth. **353** (2012) 39-4.
9. Osamu Morohara, Hirotaka Geka, Yoshitaka Moriyasu, Naohiro Kuze. Sb irradiation effect on growth of GaAs thin film on Si (111) substrate. Journal of Crystal Growth, **378** (2013) 113-116.
10. Marc J. Madou. Fundamentals of Microfabrication: The Science of Miniaturization, 2nd Ed. (2002).
11. K.Petkov, R. Todorov, D. Kozhuharova, L. Tichy, E. Cernoskova, P. J. S. Ewen. Changes in the physicochemical and optical properties of chalcogenide thin films from the system As-S and As-S-Tl. J. Mat. Sci. 2004;39:96–8..
12. E.Marquez, A. M. Bernal-Oliva, J. M. Gonzales-Leal, R. Pietro-Alcon, T. Wagner. Optical properties and structure of amorphous (As0.33S0.67)100-xTex and GexSb40-xSx0 chalcogenide semiconducting alloy films deposited by vacuum thermal evaporation.J. Phys. D: Appl. Phys. 2006; 39:1793–7.

13. Q.Lu, H.Zeng, Z.Wang, X.Cao, L. Zhang.Design of Sb2S3 nanorod-bundles: imperfect oriented attachment. Nanotechnology 2006;17:2098–7
14. Z.S.El Mandouh, S.N.Salama.Some physical properties of evaporated thin films of antimony trisulfide.J.Mat.Sci. 1990;25:1715–4.
15. Xiaojun Zhang, Kin Man Yu, Coleman X. Kronawitter, Zhixun Ma, Peter Y. Yu, andSamuel S. Mao. Heavy p-type doping of ZnSe thin films using Cu_2Se in pulsed laser deposition. Appl. Phys. Lett. **101** (2012) 042107.
16. M.T.S. Nair, Y.Pena, J. Campos, V.M Garica, P.K. Nair. ChemInform Abstract: Chemically Deposited Sb2S3 and Sb2S3—CuS Thin FilmsJ. Electrochem. Soc.1998; 145: 2113–8.
17. A. Gassoumi, M. Kanzari and B. Rezig.Thermally induced changes in optical and electrical properties of thin SnSb2S4 films. Eur. Phys. J. Appl. Phys. 2008;41:91–5.
18. O. S. Heavens, Optical Properties of Thin Solid Films, Butterworths, London; 1955.M.
19. Godlewski, E. Guziewicz, K. Kooalko, E. Lusakowska, E. Dynowska, M. M. Godlewski, E. M. Godys, M. R. Phillips. Origin of white color light emission in ALE-grown ZnSe. J. Lumin. **102–103** (2003) 455.
20. G. Landwehr and D. Hommel. Blue-Green ZnSe Laser Diodes for Optoelectronics. physica status solidi (b) **187** (2006).
21. www.kayelaby.npl.co.uk/general physics.
22. G. Grebe, G. Roussos, H.-J. Schulz. C^{r2+} excitation levels in ZnSe and ZnS. J. Phys. C: Solid State Phys. 9 (1976) 4511-4516.
23. V. D. Ryzhikov, N. G. Starzhinskiy, L. P. Gal'chinetskii, L. L. Nagomaya, P. A. Gashiu, V. P. Makhniy, G. Tamulaitis, W. Klamra, D. N. Kozin, E. A. Danshin. Properties of semiconductor scintillators ZnSe(Te,O) and integrated scintielectronic radiation detectors based thereon. Nuclear Science Symposium Conference Record **1** (2000). DOI. 10.1109/NSSMIC.2000.949152
24. Ginley, D.; Green, M.A. (2008). "Solar energy conversion towards 1 terawatt". MRS Bulletin. 33.
25. Jump up^ Andrade-Arvizu, Jacob A.; Courel-Piedrahita, Maykel; Vigil-Galán, Osvaldo (2015-04-14). "SnS-based thin film solar cells: perspectives over the last 25 years". Journal of Materials Science: Materials in Electronics. 26 (7): 4541–4556. doi:10.1007/s10854-015-3050-z.ISSN 0957-4522.

26. ^ Jump up to:[a] [b] Nair, P. K.; Garcia-Angelmo, A. R.; Nair, M. T. S. (2016-01-01). "Cubic and orthorhombic SnS thin-film absorbers for tin sulfide solar cells". physica status solidi (a). 213 (1): 170–177.doi:10.1002/pssa.201532426. ISSN 1862-6319.

27. O. Savadogo, K.C. Mandal Solar Energy Mater. Solar Cells, 26 (1992), p. 117

28. Q. Han, J. Chen, J. Lu, X. Yang, L. Lu, and X. Wang, Thin Solid Films. 62, 2050 (2008).

29. T. Ben Nasr, H. Maghraoui_Meherzi, H. Ben Abdallah, and R. Bennaceur, Physica B **406**, 287 (2011).

CHAPTER 2

2 LITERATURE SURVEY

In 2004, K.Petkov et.al. [1-4]Doped and perfectly thin film of sulfosalts are thought as well as very significant towards the employ conversion of solar energy and thermo-electrical cooling engineering's along with other photo conductive practical application. Sulfosalts have many important aspects that can be applied in many solid-state appliances. The extended technological concern in sulfosalts thin film are use in photovoltaic applications and thermos electric energy conversion.

In 2011, Kanzari et.al.[7-9] conducts with data-based investigation for checking annealing effect on sulfosalts on the structural, morphological and optical dimensions of $SnSb_4S_7$ thin films, developed using thermal vacuum vaporization method. The structural analysis reveals by XRD that the films are non-crystalline at low temperatures and shows crystalline behavior at higher temperatures. When we raised the temperature we observed the decrease in transmittance maxima of the films in the visible region and the absorption sharpness's changed to lower photo-energies. He found that $SnSb_4S_7$ have direct optical transition in films, it diminishes or reduce with heating or annealing treatment. Absorption coefficients are calculated more than 10^4 cm^{-1}. It can be finalized that $SnSb_4S_7$ films could be used in many technological applications like thin film solar cells. We believe that the atmosphere nature effects much value of the transition temperature. These determinations prove that the $SnSb_2S_4$ film may be used in lot of applications like optoelectronics. [9].

In 2013, Nisar Ali et.al.[10-11] prepared Antimony tin Sulfide thin films by thermal evaporation method having 2.65 eV direct band gap which was reduce to be 1.65 eV when annealed in the presence of air at 300 ^{0}C. The reduction of band gap is due to growth in particle size on heating. The photoconductive properties increase with heating or annealing with high temperature and changes towards a more favorable band gap with high annealing. During his work, they introduce a low cost material thin films, produced by thermal evaporation technique for solar cell practical

application. Photoconductivity response indicate the crystalline nature of the films after annealing at 150^{0}C, which was assigned to the polycrystalline type of the film. They calculated optical band gap for 150 ^{0}C annealed for 2 samples almost 1.6 eV. The transmittance for those films which are annealed at 150^{0}C was promoted along visible range but almost in the visible range of light every photon was completely captivated. When they increase tin content of the samples resistivity was felt to diminish also with raising of the annealing temperature also with high the tin content. Overall literature presented the n-type behavior at low annealing temperatures. And all these properties are demonstrating that the new less price or cost technique to make device based on Antimony Tin Sulfide films for photovoltaic applications and solar cells.

In 2013, N Ali et.al [12] reported about Sn-doped Sb^2S^3 films have been obtained with 1, 2 and 3wt.% of Sn concentration, by vacuum thermal evaporation technique. The refractive indices of the films have been calculated, and found increasing with the increasing Sn content. The analysis of absorption coefficient of the deposited thin films reveals the presence of direct optical transitions. The band gap energy for such optical transition was found to be decreasing with the increase in Sn content. Some further work is needed to improve the quality of the films meanwhile results of these thin films recommending for use as new ground materials for photovoltaic applications.

In 2013, A.Saeed et.al [13] Tin antimony sulfide ($SnSb_2S_4$) thin films were produced by thermal evaporation in vacuum on glass substrate in argon gas environment at 150°C. SEM is used for calculating average grain size which was 87.71 nm, while the crystallite size is 11.8 nm recorded by XRD. The transmittance of the thin film was so small for the range of wavelength 200-700 nm and the absorption coefficient was almost near about $4x10^5$ cm^{-1}. $SnSb_2S_4$ thin films having band gap of 2.4 eV with polycrystalline structure. These optical and structural dimensions are very encouraging because of producing absorbing coating for solar cell. Tin antimony sulfide thin films having absorption coefficient higher than 10^5 cm^{-1} which make it a good absorber of light for solar cell. The samples shows n-type conductivity having band gap 2.4 eV.

In 2013 Peiwei Hu et.al [14] synthesized conductive composite powders with Sb–SnO_2 nanoparticles surfaced on kaolinite particles having resistivity of 9.9Ω cm. The surface of kaolinite particles consists of SnO_2 x H_2O and the substitute of Sn^{4+} by Sb^{5+} or Sb^{3+} ions reduced resistivity. The surface of kaolinite was well coated with a dense, continuous and uniform Sb–SnO_2 layer. His

technique give more environmentally caring way to the normal output of various working composites from minerals. The attempt has been effectively achieved for the discovery of new absorbing layer for solar cells which may substitute the costly materials. These films were produced by thermal evaporator on clean glass slabs. The photoconductivity reaction was maximum for the annealed thin films in the NIR and visible spectrum while for as deposited film was not shown good response for this parameter. The transmittance of the annealed films decrease which is signal for making it as absorber layer. The optical energy band gap and thickness of the thin films was calculated by technique called Ellipsometry. Almost $10^5 cm^{-1}$ or greater absorption coefficient was recorded. The film thickness was almost 145nm. The band energy gap was found 1.6 eV of the annealed film which is a reserve bandgap used in solar fuel cells. He observed n-type conductivity of $Sn_2Sb_2S_5$ was also from this study.

In 2014 Junyuan Xu et.al [15] study about the morphological properties of the combinations of Tin and Tin-Antimony thin films using x-ray diffraction method and 119 Sn and 121 Sb MЄossbauer spectrographic analysis. The pure Antimony begin to discharge with the establishment of an non-crystallized phase formed in Antimony environments corresponding to those already existing in NaSb. Additionally goes on by the establishment of surrounding conditions similar to that of Na_3Sb.when charging starts, the reversible response takes place with high percentage. The charged anode have significant amount of sodium, which can describe the deficiency of recrystallization of antimony into crystalline form. The response of Tin Antimony with Na_3Sb gives a well manner crystal phase at higher temperatures (65^0C and $95\ ^0C$) while amorphous products form at room temperature. The reaction starts electrochemically, amorphization of solid-state reaction occurring at room temperature is regulated by the instantaneous formation of sodium coordinated tin and antimony environments, as supervised by the decrease or increase of the 119 Sn (121 Sb) MЄossbauer shifting of isomer. The lack of full sodiation of tin surroundings is proposed by a 119 Sn shifting of isomer lower than those evaluated for tin thin films or $Na_{15}Sn_4$ chemical compound. Furthermore, the comparatively large 119 Sn quadruple classifying values confirm the establishment of nano sized fields with a wider spreading of coordination than in NaSn model chemical compounds. The 119 Sn and 121 Sb shifting of isomer values further endure the absence of full sodiation of SnSb throughout charging, in agreement with the reversible content obtained throughout the electrochemical calculations.

A proton and an electron consisting of tin oxide with doped Sb supports as a conducting composite and tin pyrophosphate was checked and characterized by SEM, FTIR, XRD and conductivity tests at different temperatures. The supporting composite showed values of 0.56 S cm^{-1} at 130 ^{0}C mean conductivity under the vaporize atmosphere of H_2O, to which the conduction of proton causing a substantial involvement. Nanoparticle catalysts of Iridium oxide were developed with many kinds of supports admitting this compound with all protonic and electronic conductivities. The specially designed mass catalytic action, as evaluated in phosphoric and sulfuric acid electrolytes, were detected to higher in the rate of IrO_2 < IrO_2/SnO_2 < $IrO_2/SbeSnO_2$ < $IrO_2/SnPe(SbeSnO_2)$. Significant advancement in the kinetics of anodic water electrolysers functioning at both 130 °C and 80 °C was reached with the IrO_2 Nano catalyst confirmed on this composite compound.

2.1 References

1. K.Petkov, R. Todorov, D. Kozhuharova, L. Tichy, E. Cernoskova, P. J. S. Ewen. Changes in the physicochemical and optical properties of chalcogenide thin films from the system As-S and As-S-Tl. J. Mat. Sci. 8, 39-96 (2004).
2. E. Marquez, A. M. Bernal-Oliva, J. M. Gonzales-Leal, R. Pietro-Alcon, T. Wagner. Optical properties and structure of amorphous (As0.33S0.67)100-xTex and GexSb40-xSx0 chalcogenide semiconducting alloy films deposited by vacuum thermal evaporation.J. Phys. Appl. Phys. **39,** 1793 (2006).
3. Q.Lu, H.Zeng, Z.Wang, X.Cao, L. Zhang.Design of Sb2S3 nanorod-bundles:imperfect oriented attachment. Nanotechnology **17,** 2098 (2006).
4. Z.S.El Mandouh, S.N. Salama .Some physical properties of evaporated thin films of antimony trisulfide.J.Mat.Sci. **25**, 1715 (1990)
5. H. Dittrich, A. Bieniok, U. Brendel, M. Grodzicki, D. Topa, Thin Solid Films 515 (2007) 5745.
6. M.Y. Versavel, J.A. Haber, Thin Solid Films 515 (2007) 5767.
7. A. Rabhi, M. Kanzari *, B. RezigA. Rabhi, M. Kanzari *, B. Rezig 2008
8. A. Gassoumi, M. Kanzari, J. Optoelectron. Adv. Mater. 11 (4) (2009) 414.
9. A. Gassoumi, M. Kanzari, B. Rezig, Eur. Phys. J. Appl. Phys. 41 (2008) 91.
10. Ali N, Iqbal MA, Hussain ST, Waris M, Munair SA. Optoelectronic properties of cadmium sulfide thin films deposited by thermal evaporation technique. Key Eng Mater 2012;510–511:177–85.
11. Ali, N., Ali, Z., Akram, R., Aslam, A., Chaudhry, M. J. M. N., Iqbal, M. and Ahmad, N., Study of Sb28.47Sn11.22S60.32 Compound as thin film for photovoltaic applications.Chalcogenide letters 9(8), 329 (2012).
12. Ahmad Saeed, Nisar Ali*, Waqar a. a. syed, Photovoltaic Effect In The Metal Based Sulfosalt Thin Film Deposited By Physical Vapor Deposition Technique
13. Peiwei Hu, Huaming Yang * Controlled coating of antimony-doped tin oxide nanoparticles on kaolinite particles(2013)
14. Loïc Baggetto a, *, Hien-Yoong Hah b, c, Jean-Claude Jumas d, Charles E. Johnson b,Jacqueline A. Johnson c, Jong K. Keum e, Craig A. Bridges f, Gabriel M. Veith a,(2014)

15. Junyuan Xu a,b,c, Qingfeng Li c,*, Martin Kalmar Hansen c, Erik Christensen c,Antonio Luis Toma´s Garcı´a c, Gaoyang Liu a,b, Xindong Wanga,b,**, Niels J. Bjerrum c(2014)

CHAPTER 3

3 EXPERIMENTAL SETUP AND WORK

3.1 Thin Film Deposition

Thin film deposition involve four main stages

i.Creating vapor phase.

ii. Taking atoms or molecules from the objective material to the surface of the targeted area.

iii. Deposition of atoms or molecules on the glass substrate.

iv. Rearranging of atoms of the deposited glass to attain preferred properties.

We work in four stages:

1st stage contains all the methods which are essential for the creation of the vapor phase from the condensed state. Some typical methods are the thermal evaporation, e-beam evaporation, sputtering etc.

2nd stage the atoms in the form of vapors are transported from the target material and adsorbed on to the substrate. Some techniques such as electron cyclotron resonance plasma helped growth and activated reactive evaporation are used to control the motion of the evaporated species before they deposit onto the substrate.

3rd stage, the evaporated atoms are deposited on the substrate. Epitaxial growth of the films is a major area of thin film technology which is concerned to give an exclusive control on the composition, structure and defect free growth of the film.

4th stage, the rearranging of the atoms or reconfiguring the surface morphology of the film takes place to give the preferred properties for the product. Formation of a thin film begins via nucleation and growth processes [1]. Step-by-step growth operation can be showed as under:

The vapors on hitting the glass surface lose some portion of velocity and are accumulate onto the glass surface. Initially accumulated atoms being not in thermal equilibrium with the substrate keeps on changing their position over the substrate surface. The adsorbed atoms interact between themselves, forming bigger nuclei. These appearing nuclei are thermodynamically unstable and have a tendency to desorb. If the deposition factors are controlled in an optimum style such that other adsorbed species strikes nuclei prior to getting desorbed, it begins to grow in size. After attaining a confident critical size, the nuclei become thermodynamically stable and this step is called the nucleation stage. The highest nucleation density is achieved when number of critical nuclei grow in reasonable dimension until a saturation point reached. The size of nuclei and the nucleation density depend upon a number of components such that energy of activation of the adsorbed element, substrate temperature, and the magnitude of impingement and chemical/physical nature of the substrate. Nuclei can grow on the substrate in two ways: either by diffusion of the adsorbed species parallel to the surface of substrate by or vertical to it by direct collision of the incoming species. The grown-up and mature nuclei are called islands.

In the next level, these formed islands start coalescing with each other to decrease the substrate surface area in the progression of film formation. At this stage the formation of bigger islands is enhanced by increasing the substrate temperature thus increasing the surface mobility of the adsorbed species and agglomeration is assumed to happen. [2-3].

3.2 Thin Film Deposition Techniques

In most of the literature, generally the establishment of thin films is classified into two main classes

i. Deposition by physical process

ii. Deposition by Chemical vapor Process

In chemical vapor deposition process, the film composition varies from that of the target material whereas, in deposition by physical vapor process the deposited material have the similar composition just like source material. In general, physical deposition methods are very common either regarding the material to be deposited or to the particular substrate. There are lot of techniques that use the both processes. A list of different techniques is given below.

3.2.1 Chemical Vapor Deposition

Here, a precursor in fluid form goes through a chemical change at the substrate surface, parting a solid layer. The fluid tends to surround the solid film, deposition occurs on the surface, with a very minute consideration to direction. Thin films deposited by CVD techniques tend to be conformal, rather than directional. CVD normally uses a gas precursor, generally a hydride or halide of the material to be fabricated. In MOCVD, metal-organic gas is used. Some of the commonly used CVD techniques are:

a) Plasma enhanced (PE) CVD

b) Plasma polymerization

c) Deposition by Chemical vapor method

d) Chemical solution deposit method

3.2.2 Deposition of Physical Vapor Process

Deposition by Physical vapor process utilizes mechanical ways to fabricate a thin film of target material. The target material is positioned in an energetic and high vacuum chamber so that vapors of material can run away the surface. The whole deposition process is done in a vacuum environment, to allow the particles to travel without any restriction. In this way, the vapors follow a straight path and the deposited films are directional.

PVD has three fundamental steps to deposit a thin film. First solid target material is sublimated to vapors; Secondly, atoms in vapor state passes through the vacuum to the substrate surface. Lastly, target material is deposited onto the glass surface to develop an optical thin film. Some of the commonly used PVD techniques are:

a) Sputtering

b) Deposition by Pulsed Laser

c) Molecular Beam Epitaxy

d) Thermal Evaporation

The technique which I have used to deposit the films is close spaced sublimation technique. It is one of the types of thermal evaporation technique so we concentrate on this particular technique.

3.2.3 Close spaced sublimation (CSS)

Sublimation by Close spaced is a case of thermal vaporization. It is an old PVD technique commonly used for coating technology in decorations and wear resistance applications [12]. In this technique the target material is placed in a boat of resistive element such as tungsten, molybdenum and tantalum etc. A very high direct current is allowed to pass in these boats with very low voltage. The melting point of resistive boats is very higher than the objective materials, therefore the material is vaporized and deposited on the substrate surface by producing joule heating effect. The target material and substrate are closely spaced usually just a few mm apart. The target material can be of any shape according to requirement.CSS is widely used in the manufacturing of microelectronics and in the research labs making the most efficient II-VI compound semiconductor solar cells.

This project consists of two phases: In the first phase we have prepared the thin films by physical mixing and then its micro or nano-films were developed on a glass thin film by utilizing two source sublimation method. In the second phase these annealed and as-deposited samples were characterized with by using different diagnostic tools. For compositional analysis Rutherford backscattering spectroscopy (RBS) has been employed. X-Ray diffraction (XRD) were utilized for the structural analysis whereas for optical analysis spectroscopic ellipsometer was used.

3.3 Two Source Sublimation Technique

Thin films of antimony sulfide with tin doped have developed on glass micro sized slab at room temperature by thermal evaporation technique. Thermal evaporator is use for doping during two source sublimation technique to look into its effects on structural, electrical and optical properties of Sn-doped Sb_2S_3 thin films.

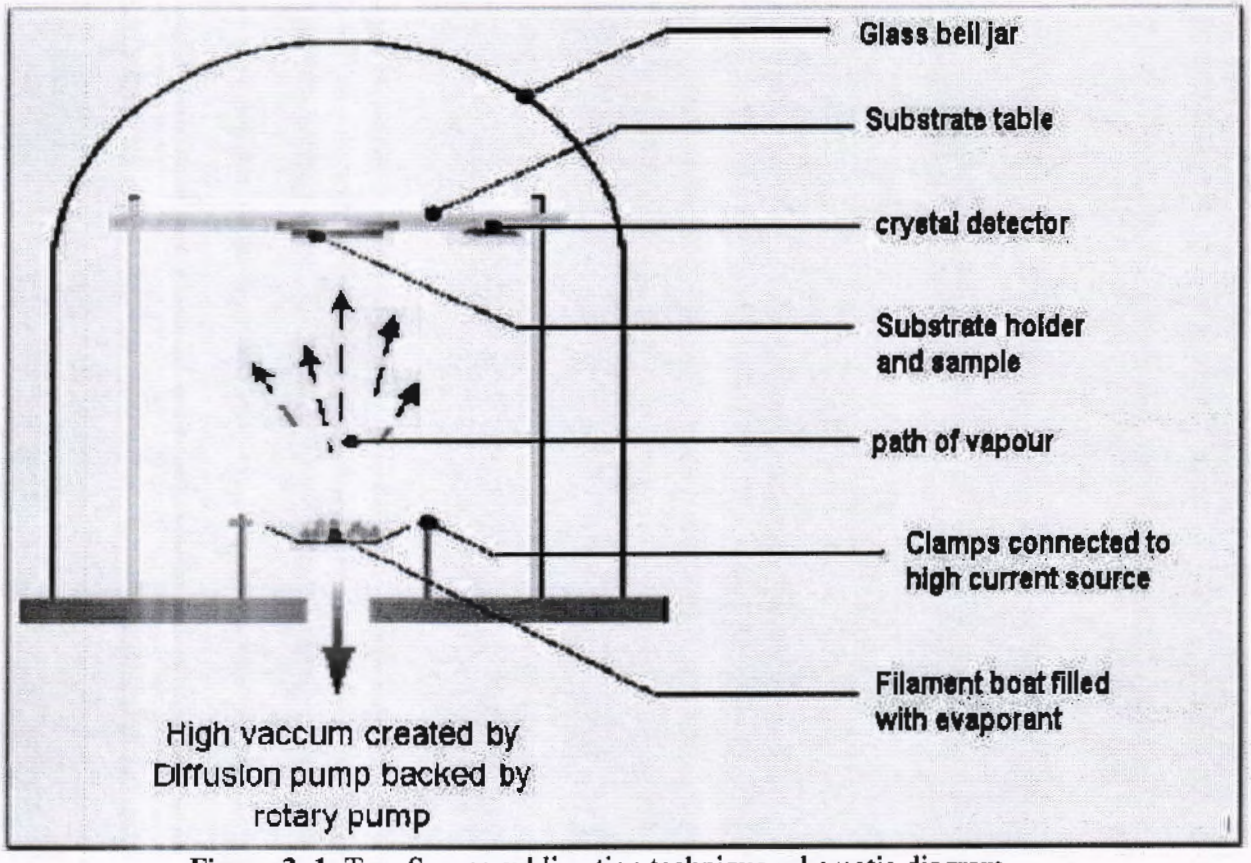

Figure 3. 1: Two Source sublimation technique schematic diagram.

The main constituents of the experimental arrangement are given below

i. DC power supply
ii. Vacuum chamber
iii. Substrate holder
iv. Optical films thickness monitoring by monochromatic light system.
v. Rotary and diffusion pumps for vacuum creation
vi. heating plant
vii. Cooling system (chiller)
viii. Resistive boats such as tungsten, molybdenum etc

The experimental set up is shown in Figure. 3.2

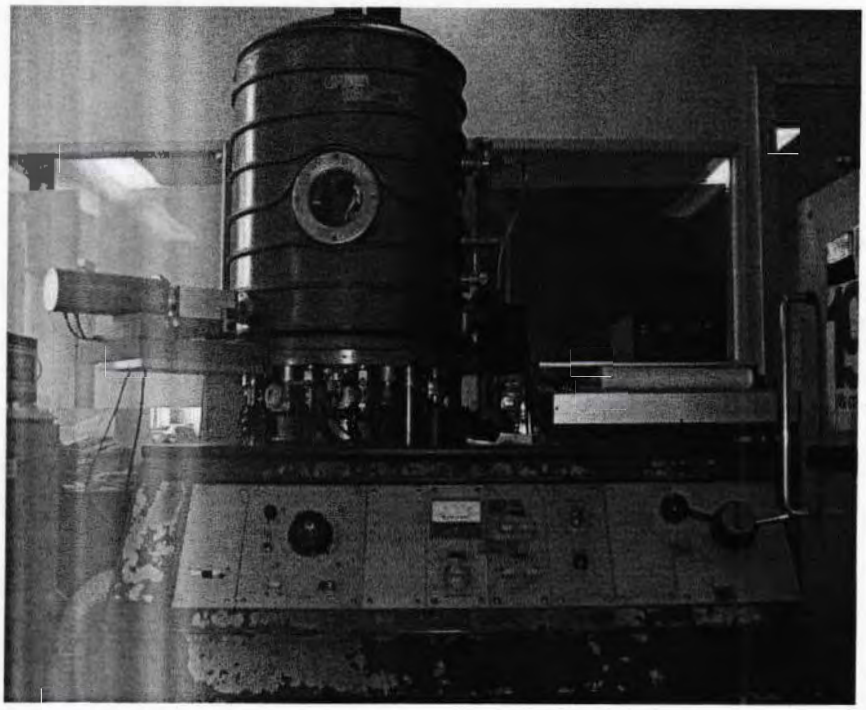

Figure 3. 2: Experimental set up of close spaced sublimation Chamber

3.4 Deposition of SnS with Sb_2S_3 on thin films using Evaporation method

Sb_2S_3 films were produced on glass micro sized slab by two source evaporation method at room temperature. A vacuum coating unit along with diffusion pump is already installed. Almost $2.6665x10^{-3}$Pa pressure inside the chamber during the whole process. We use fine grinded powder of Sb_2S_3 along with SnS with 99.9% purity. Then after vaporization of these powders were deposited on the neat glass substrates at room temperature by two source method. The time for deposition of samples is almost 5-7 minutes and compositions for all samples were deposited under similar conditions.

3.4.1 Deposition parameters

- Substrate temperature = Room temperature
- Chamber pressure $\approx 10^{-5}$mbar
- Current = 30-40 Amperes
- Deposition Time = 26-28 minutes
- Deposition rate $\approx$ 0.2 nm/sec

3.5 Characterization Techniques Used for Tin Antimony Sulfide Thin Films

1. Rutherford backscattering spectroscopy (RBS)
2. PIXE
3. Scanning Electron Microscopy (SEM)
4. X-ray Diffraction (XRD)
5. Ellipsometry
6. Hall measurement

3.5.1 Rutherford Backscattering Spectrometry (RBS)

Rutherford Backscattering Spectrometry is a well depicted, analytical, non-destructive, quantitative and a fundamental investigational tool. For material examination, it is distinctive technique generally used in thin films for thickness, depth profiling of basic elements and elemental composition. Generally, for incident protons and He^{+} ions, analyzed depth is nearby 20 μm and 2 μm, respectively [4-5]. In RBS technique a beam of He^{+2} or H^{+} (protons) bearing energy normally 4 MeV to 0.5 is incident On a stable target. Backscattered ions are collected on silicon detectors. Energies are depended on the characteristics of target atom, depth into target sample up to which particles penetrate and scattering angle before scattering. Hence, RBS can be used for elemental analysis [6]. For first time in 1957 by Rubin et al. RBS was described as an experimental setup for material analysis and has since originated into main materials characterization method [2, 7]. RBS is a fast valued technique which does not need any mention standards, non-destructive and multiple elemental analysis technique for the elements (Beryllium to Uranium) [3]. Typically prominent accuracy up to ± 3% and have a deepness up to almost 2 - 10 nm [11]. Detection limit is about ~ 10^{18} cm^{-3} but RBS sensitivity in case of heavier elements is almost 100 ppm so it is not good for revealing lighter elements [4, 11]. Size of the beam spot varies from 0.5 - 2.0 mm [3]. The schematic diagram of RBS as experimental setup is shown in Fig. 3.3.

3.5.1.1 Instrumentation

Rutherford Backscattering Spectrometry (RBS) technique can be done through an experiment using ion beam analysis (IBA) device, which consist of mainly three portions,

i. linear particle accelerator
ii. ion source
iii. Particle detector [3]

All these collection of components is expressed in Figure. 3.3.

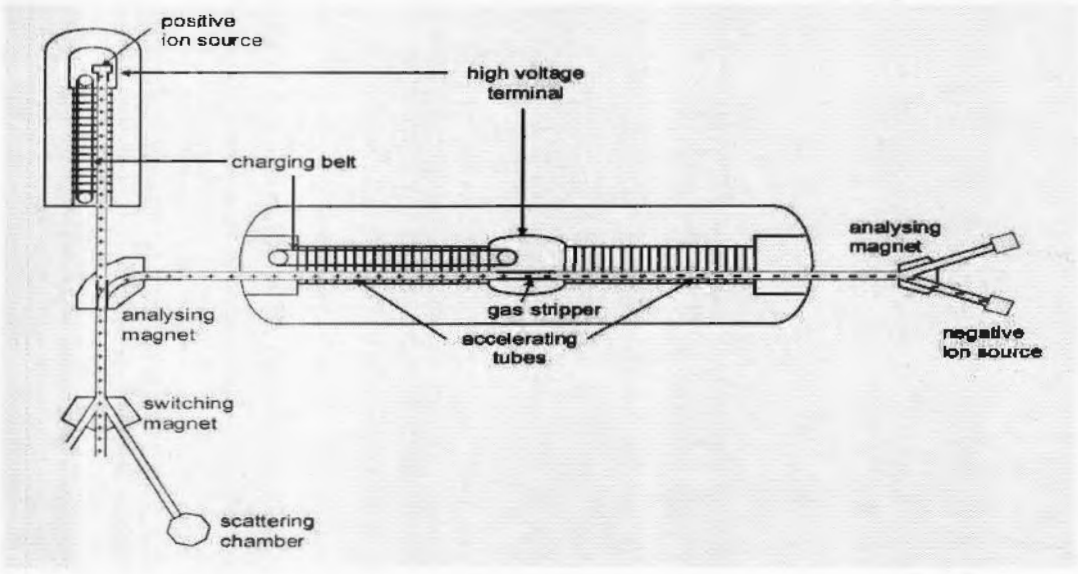

Figure 3. 3: Schematic of RBS instrument

3.5.1.2 RBS Experimental Setup

RBS analysis was performed using **"Tandem Pelletron Accelerator** facility at National Centre for Physics (NCP), Data Analysis Lab, Islamabad" as shown in Figure. 3.4. The samples were illuminated by well collimated beam of He^{+} 2mm diameter and energy of 2.023 MeV. The sample was fixed in a vacuum chamber on a five-axis adaptable goniometer with an accuracy of 0.01°. The backscattering ions were logged by a surface barrier detector at an angle of 170° and energy resolution 25.8 keV. A beam integral connected with the sample frame was used to make sure that the tests are repeatable, comparable and acceptable charge on sample.

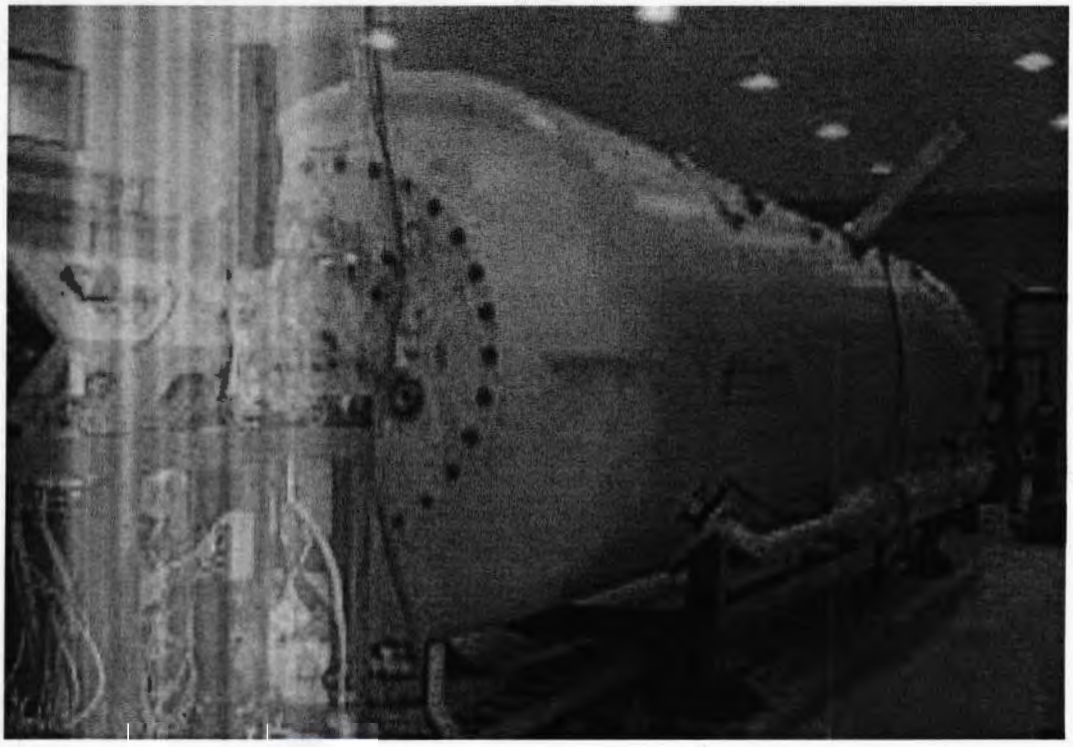

Figure 3. 4: A 5UDH-2 Pelletron Tandem Accelerator at NCP, Islamabad.

3.5.2 Proton Induced X-Ray Emission (PIXE)

Elemental composition of a sample material is calculated by Proton Induced X-ray Emission (PIXE). When ion beam is directed towards a sample displayed in front of beam, some interactions happened that give off electromagnetic radiations of wavelengths (λ) in x-ray region. PIXE technique is non-destructive, compositional analysis is used normally by archaeologists, scientists and also useful for place of origin, dating and validity.[8].

The schematic diagram of the instrument is given in figure 3.5

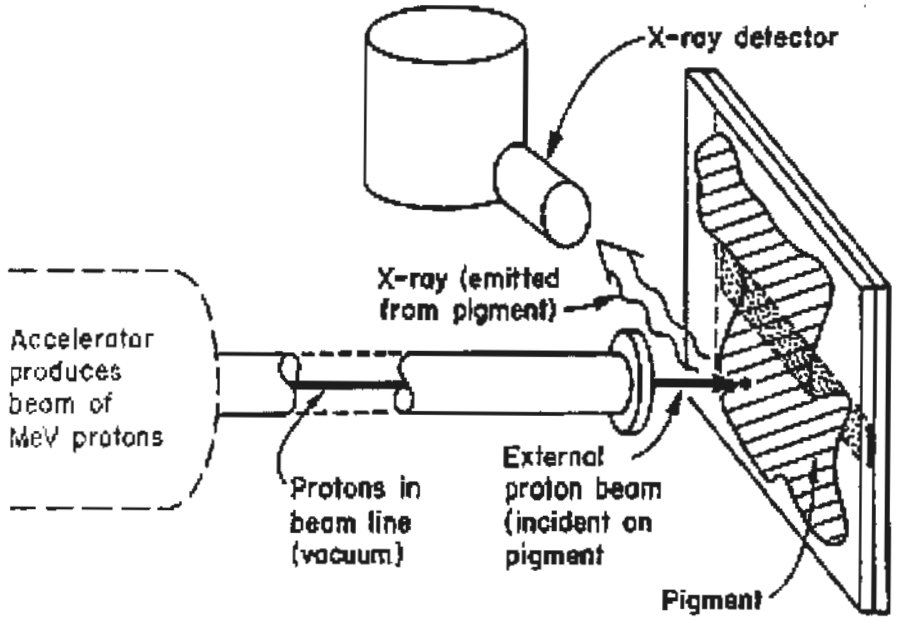

Figure 3. 5: Schematic diagram of PIXE

3.5.2.1 The Benefits of PIXE:

i. Matrix composition, detector efficiency, and peak overlap all are the important factors for absolute trace sensitivity for given trace element.

ii. Material investigations can be done for any material from normally uranium to sodium in a single spectrum on our arrangement. The materials are bombarded with protons, and x-rays that are produced by the interaction between the sample atoms and protons.

iii. When we starts the experiment apply a high vacuum environment in detector. The presence of air might be reduce the functioning of detector. Meanwhile, with the addition of Helium we reduce this effect.

3.5.3 X-Ray Diffraction (XRD)

XRD is normally used to examine the material structure of thin solid films and bulk including lattice constants, orientation of crystals, and preferred orientation of poly-crystals, surface and inner defects, grain size, strain, stress etc. It is a nondestructive technique and do not require

complicated sample preparation or conducting film at the substrate. X-Rays of few angstroms which is about 1.54Å in wavelength is used and have a diffraction spectra 2Θ scanning mode ranging from 10 to 90 degree diffraction angle. X-Rays are produce when a fast cathode (electron) strikes with tungsten in the result of this bombardment produced x-rays fall on the sample which is under observation. Rays striking with samples penetrate deep inside the sample and reflect back, these reflected rays detected by a high efficient detector and give us structural information.

Interference of the diffracted waves from dissimilar planes of atoms takes place giving a diffraction pattern. These diffraction patterns yield sharp interference peaks where the atoms are fixed up in a periodic manner. Bragg's law is used to detect the circumstance for a diffraction peak to take place.

$$2d\sin\theta = n\lambda \quad \text{.....(3.1)}$$

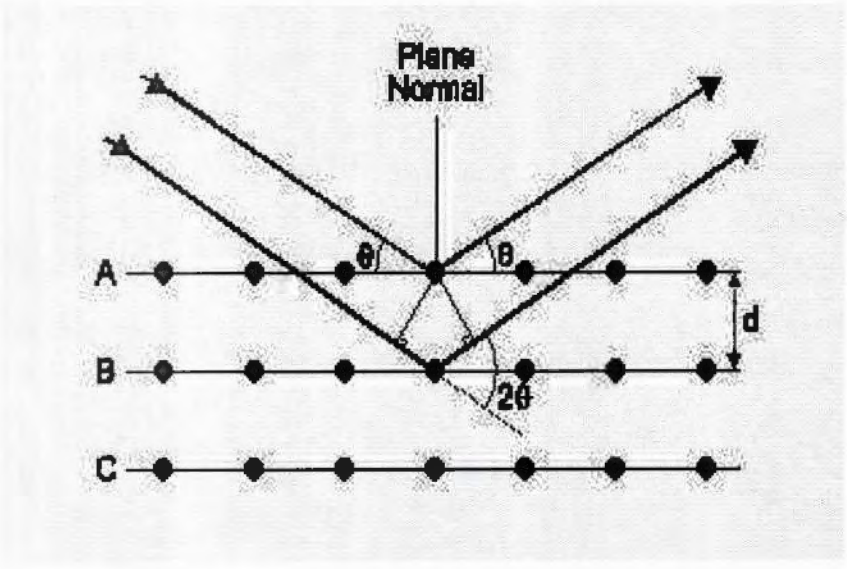

Figure 3. 6: Bragg's diffraction

Where scattering angle θ, inter-planar distance d where order of the diffraction peak is representing by n, wavelength of the x-ray radiation λ as shown in Figure. 3.5. The snap of the XRD apparatus is shown in Figure. 3.6.

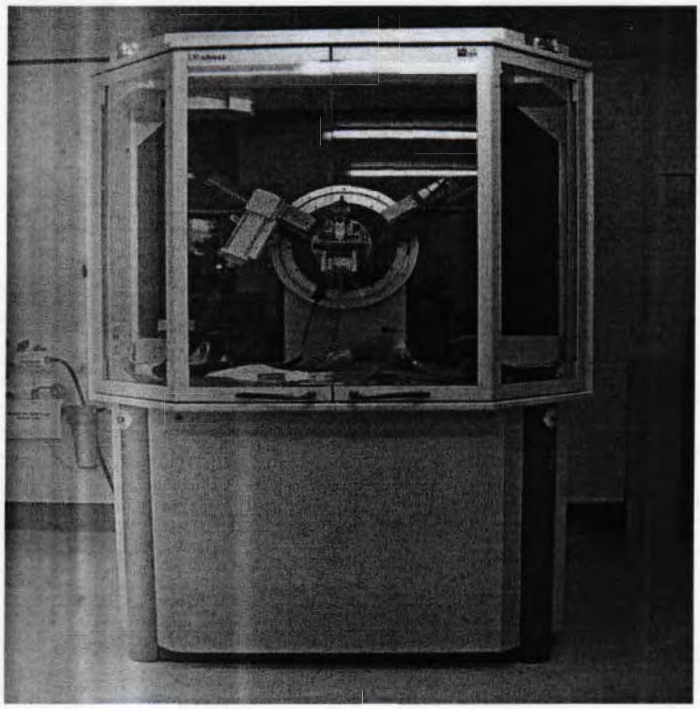

Figure 3. 7: (XRD) X-ray diffraction machine

A significant appliance of x-ray diffraction is to attain an approximate of the grain size. This is very helpful as many material properties depend significantly on crystallite size [40, 41]. The thickness't' or grain size may be calculated by means of Debye-Scherer relation 3.2

$$t = \frac{K \times \lambda}{B \times \cos\theta_B} \quad \text{.....(3.2)}$$

Where K is a constant depending on crystalline shape having value 0.9, wavelength of X-rays λ, ß is Full Width at Half Maximum (FWHM) and θ_B is the Bragg angle. And by Scherer relation, the particle or grain size is inversely proportional to the broadening of peak. There are different reasons of peak broadening e.g. strees/strain developed in the films or the instrument used.

3.5.4 Spectroscopic Ellipsometery (SE)

Ellipsometry is employed to characterize thin films microstructure, optical and dielectric constants and surface roughness. SE is very sharp measurement method that uses polarized light. Reflected polarized light change its phase in a beam which drives its sensitivity. SE is a non-contact and non-

destructive method and no vacuum is required. No need of standards or reference because ellipsometry is an absolute method. It provides twice more information (both amplitude and phase ratio) than reflectometry (only intensity). In addition, as ellipsometer does not deals with the intensity but with polarization state so it is less sensitive to fluctuations in light intensity. For thin film characterization hence it is the best non-destructive technique. Both imaginary and real part of the complex refractive index dielectric function can be obtained. The film thickness can be calculated with great accuracy.

3.5.4.1 Ellipsometer Measurements

Through the surface of sample, ellipsometry find the transmittance or reflectance change in polarization state of light. Basically, ellipsometry concern only to extent of polarization state of light beam. Nevertheless, polarization state of a beam of light modifies by optical system are usually measure by the ellipsometery. Optical system is simply the sample, for thin film analysis. The calculated values are delta (Δ) and psi (ψ). All these values are associated to the ratio of R_s and R_p (Fresnel coefficients of reflection) for s and p polarized light.

$$\rho = \frac{R_p}{R_s} = \tan(\psi)e^{i\Delta} \qquad \text{..... (3.3)}$$

Ellipsometery is very reproducible and highly accurate because it calculates the ratio of two values. This ratio also contain phase information and is complex number that's why the measurement very perceptive.

3.5.4.2 Parameters Determined by Ellipsometer

To characterize both bulk materials and thin films ellipsometry is usually used. Thin film optical constants and thickness are most common measurements. It is also the major technique for finding optical parameters in IR, Visible and UV wavelength ranges. Ellipsometry is very sensible and compromising technique in many material properties. Various parameters such as reflection, transmission, absorption, optical constants, doping concentration, thin film thickness and crystallinity etc. can also be measured by ellipsometry.

The schematic diagram for ellipsometry is shown Figure 3.6. We use the light which is monochromatic, collimated, and then linearly polarized. Upon transient by the compensator (generally a quarter-wave plate), circularly polarized is obtained and then specimen surface is

illuminated. The light is transmitting through a following polarizer after reflection, which serves as the analyzer. Lastly, the light intensity is calculated quantitatively by a detector (photomultiplier) or judged by eye. Until light extinction occurs the analyzer and polarizer are rotated. The amplitude ratio of the two components of reflected light determined the phase difference. From these, either the refraction index or thickness of material can be obtained. The schematic diagram of the ellipsometry arrangement is shown in Figure 3.7.

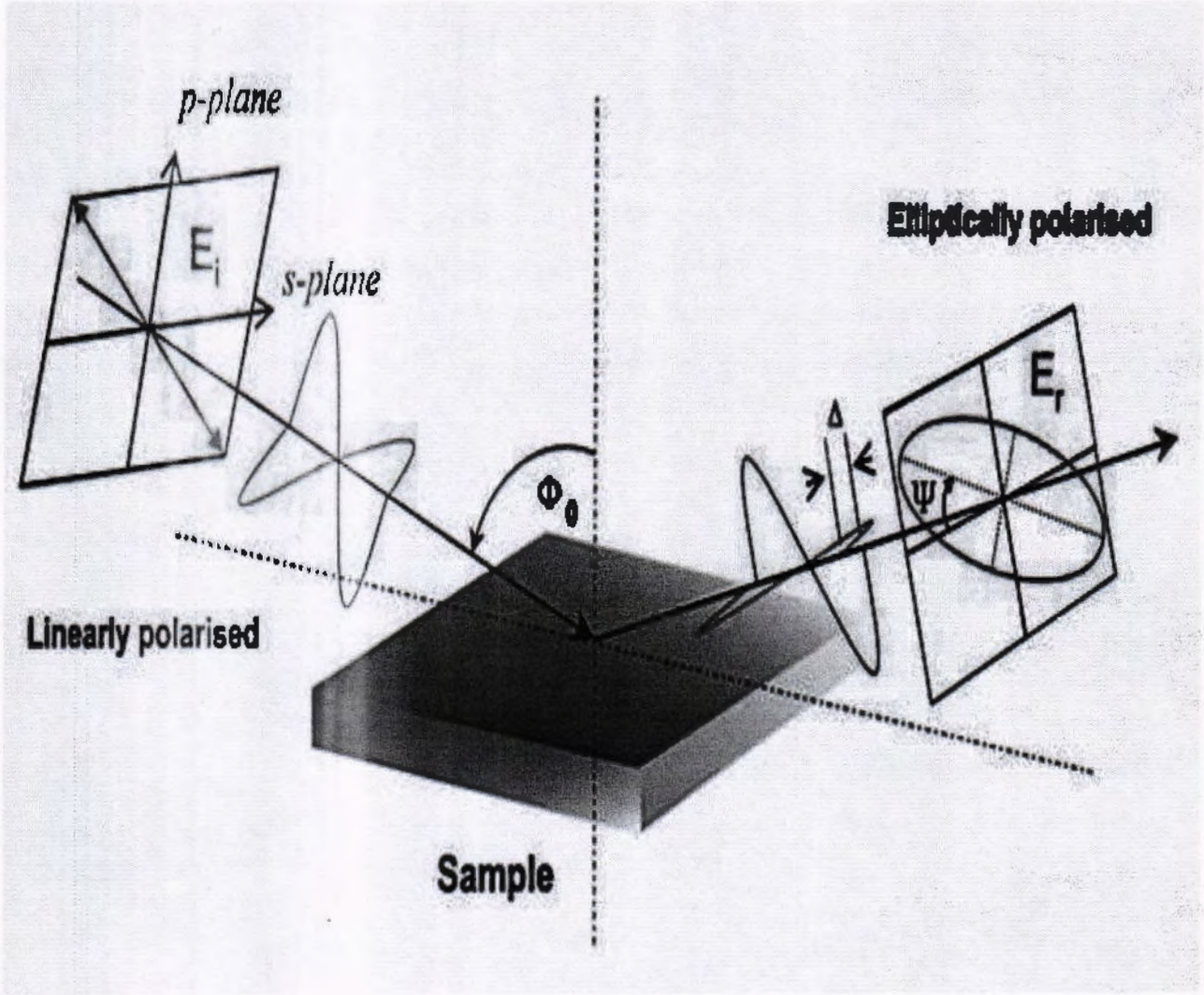

Figure 3. 8: Schematic diagram of spectroscopic ellipsometry technique

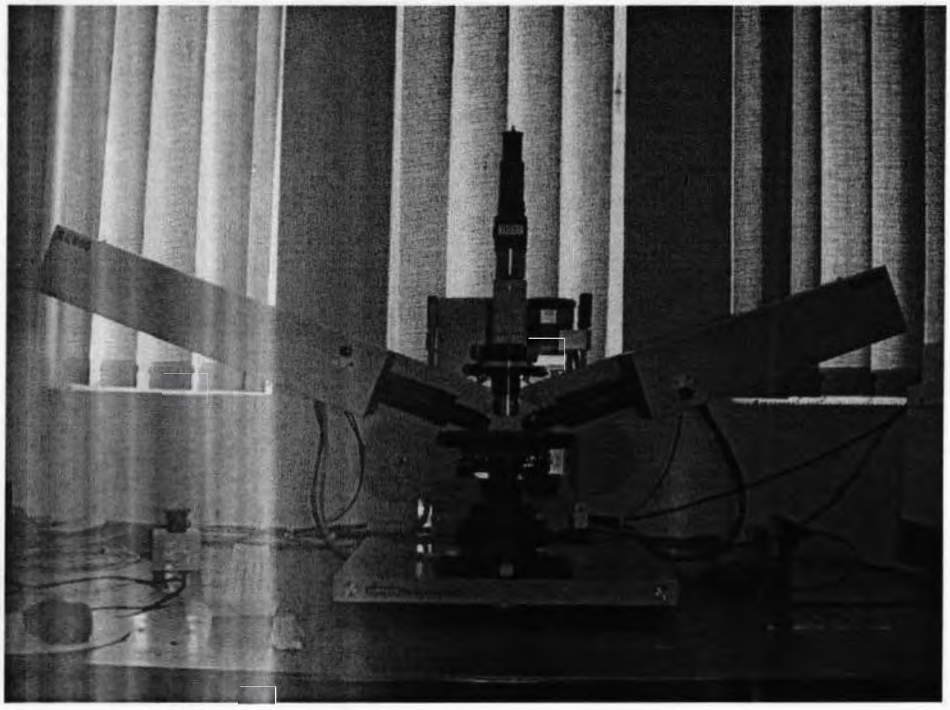

Figure 3. 9: Spectroscopic ellipsometry system at IIUI

3.5.4.3 Methods in Ellipsometry for Data Analysis

Obtain Ψ and Δ (phase and amplitude changes) data versus angle of incidence and wavelength. Formulate an optical model that describe as much as possible the information about sample structure. All layers in the sample structure must be counted. Create (simulate) an optical model by which theoretical data obtained must match to the data obtained experimentally and compare them. Unknown parameters such as optical constants or thin film thickness or both in the optical model are varied until "best fit" to experimental data. To vary unknown parameters regression algorithms are used and reduce the difference between the experimental and generated data. Once a good "fit" to the experimental data is achieved, sample's physical parameters such as optical constants, film thickness, surface roughness, composition etc are obtained.

There are two types of energy band gap (E_g).

- Indirect Band Gap
- Direct Band Gap

We can determine optical band gap (E_g) by help of the Kabulka-munk and the tauc plot method.

The Kubelka-Munk equation at any wavelength is

$$F(r) = \frac{(1-r)2}{2r} \quad \text{..... (3.4)}$$

Where reflectance r and F(r) is so called Kubelka-munk function.

Tauc plot relation is given below;

$$(\alpha h\upsilon)^{1/n} = A(E_g - h\upsilon) \quad \text{..... (3.5)}$$

Where "α" is coefficient of absorption, "h" is planks constant and its value is "6.62×10^{-34} m^2 kg / s", "υ" is the frequency of incident radiation. "E_g " is the band gap energy and "A" is a constant. "n " is constant and its value depends upon the type of band gap.

The energy of incident radiation is determined by this relation;

$$E = \frac{hc}{\lambda} \quad \text{..... (3.6)}$$

a. Direct Band Gap

According to electronic band structure of solids, band gap can be defined as the difference of energy between valance and conduction band. So minimum and maximum energy of conduction and valance band respectively lies on the same vertical energy axis in direct bandgap. In such situation, an electron lying in the conduction band can fall freely into a hole in the valance band. Either by itself or by the action of the external electric field without changing its momentum. For the direct band gap the value of "n" in the tauc plot relation is "1/2" so equation (3.5) becomes,

$$(ahv)^2 = A(E_g - hv) \quad \text{..... (3.7)}$$

b. Indirect Band Gap

This type of band gap has minimum energy of conduction band and maximum energy of valance band lies on different vertical energy axis. Its means a conduction band electron cannot fall into a valance band hole without changing its momentum.

For Indirect band gap the value of "n" in the tauc plot relation is "2" so equation (3.5) becomes,

$$(ahv)^{1/2} = A(E_g - hv) \quad \text{.....(3.7)}$$

The refrective index "n" of thin films is clculated by by the following relation :

$$n = \frac{([N + (N^2 - 4s^2)^{(1/2)}])}{2} \quad \text{.....(3.8)}$$

"s" is the substrate's refractive index and "N" is the no of oscillations.

"N" is obtained by following relation:

$$N = 1 + s^2 + 4s(\frac{T_M - T_m}{T_M T_m}) \quad \text{.....(3.9)}$$

"T_M" and "T_m" is the transmission maxima and minima respectively.

Thickness of film can be obtained by using this formula:

$$d = \frac{1}{4n}[\frac{\lambda_m \lambda_M}{\lambda_M - \lambda_m}] \quad \text{.....(3.10)}$$

Thickness of the film (d) is equal to, (λ_M) maximum value of the wavelength, "λ_m" is minimum value of the wavelength and "n" is the refractive index of thin film.

The dielectric constant, band gap energy (E_g), film thickness and of the deposited films were measured by an ellipsometer (J.A. Woolam M-200VI). At an incidence angle of 70° the experimental delta (Δ) and psi (Ψ) spectra were recorded.

3.5.5 Scanning Electron Microscopy

SEM is the powerful tool for the characterization of nanomaterials. Scanning electron microscopy is a tool for observing the surface morphology, crystallography and orientation of grains of the material. This technique is used to study thin films surfaces and sensing layers. The scanning electron microscopy (SEM) is used at micro level scale and it is a versatile tool for the study of surface of the material. Secondary electron images of organic and inorganic materials were obtained by SEM with nanoscale. SEM also provides the high resolution of the material up to nm scale and magnified the image up to 50000X. In SEM we apply electron beam instead of the light. The principle on which SEM works depends on the momentum transfer. When we shoot high energy electrons to the target samples then we examine the emitted electrons or photons and

x-rays. The incident electron beam is spread out at the sample in both elastically and in-elastically ways.

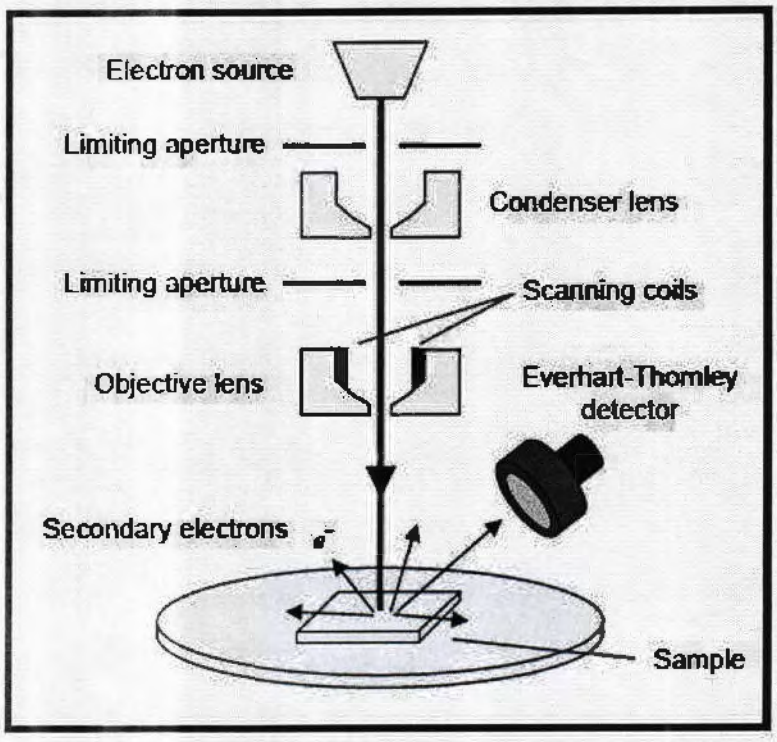

Figure 3. 10: Schematic diagram of SEM

When the incoming beam of electrons are contact with the target samples then it radiates the secondary electrons, X- rays and the back-scattered electrons. The secondary electrons are made from the interaction between the incoming electrons and outer electrons. The secondary electrons have low energy about 10 to 50 eV as compared to the back-scattered electrons. The secondary electrons cast their energy when they come out from the target material. The no. of secondary electrons is higher than the no. of incoming electrons. SEM experimentation worked properly when the samples must be conductive. If the target material is not conductive then the samples are coated by a conductive layer. During the electron bombardment the access of charges from the surface is grounded by using conductive layer. Elemental composition is obtained by the emitted x-rays from target samples. [20]

3.5.6 Hall measurement

Hall Effect measurements are used in different phases from basic materials to device manufacturing. Crystal's industry also use this technique, as researchers do in university and industrial based labs.

A Hall Effect observation system can be used to measure few material parameters, but primary is the Hall voltage (VH). Other important parameters such as carrier mobility, Hall coefficient (RH) magnetoresistance (R), carrier concentration (n), resistivity and the conductivity type (N or P) are all obtained from the Hall voltage.

With the addition of some other devices, I-V characterization results can be generated with a similar setup. Hall measurements are beneficial for characterizing every material used in developing semiconductors, such as germanium and silicon, as well as most compound semiconductor materials, including silicon-carbide (SiC), silicon-germanium (SiGe),gallium arsenide (GaAs), indium arsenide (InAs), aluminum gallium arsenide (AlGaAs), indium gallium arsenide (InGaAs), cadmium telluride (CdTe), indium phosphide (InP) and mercury cadmium telluride (HgCdTe).

By using the following equation we can find the Hall voltage (Vh) across the conductor.

$$V_h = \frac{IB}{dne} \quad \text{.....(3.11)}$$

Where 'B' is magnetic field, 'I' is current across the conducting plate, 'e' is electron charge, 'd' represent the depth of plate and 'n' denotes the charge carrier density.

The hall coefficient of is described at the same time as

$$R_h = \frac{E_y}{j_x B} \text{.....(3.12)}$$

Where 'j' is current density of the carrier electrons and 'E' is the induced electric field.

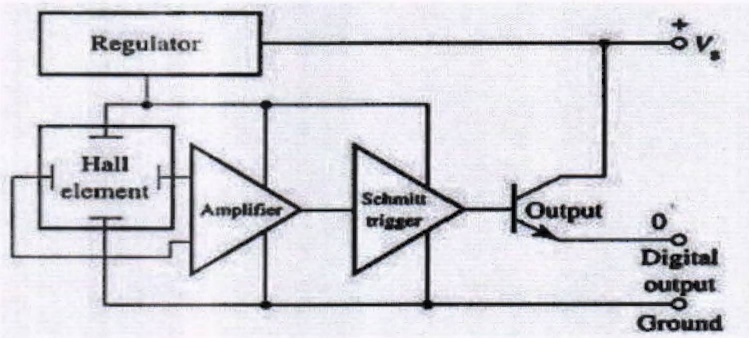

Figure 3. 11: Hall schematic diagram

I. Mobility(μ)

Hall mobility is defined as the resultant product of the conductivity (Λ) and the Hall coefficient (R_H)

$$\mu = R_H \sigma \quad \text{.. (3.13)}$$

The expression for the Hall coefficient is defined over, wherever as resistivity (ρ) is the inverse of conductivity (σ). Resistivity is given as

$$\rho = \frac{RA}{L} \quad \text{.. (3.14)}$$

Where 'A' is area and 'L' is length of the sample.

There are two types of doping (n-type and p-type) which can also be tested by Hall effect. It can be checked by the sign of Hall voltage, if the voltage is positive the material is p-type and if voltage is negative the material is n-type.

II. Resistivity (ρ)

The electrical resistivity is defined as the resistance of rectangular shape of a thin film at constant temperature is given by

$$R = \frac{\rho l}{db} \quad \text{.. (3.15)}$$

Where 'ρ' is the resistivity,'d' is the thickness , 'd' and 'b' is the length and width of the rectangular sample.

3.6 References

1. M. Ohring. The material science of thin films. San Diego New York (1992).
2. ETAFILM Technology. www.etafilm.com.tw. Chungli Ciy. Taoyuan Hsien 320. Taiwan.
3. W. D. Nix and B. M. Clemens Crystallite coalescence: A mechanism for intrinsic tensile stresses in thin films. J. Mat. Res. 14 (1999) 3467-3473.
4. M. Mayer. Rutherford Backscattering Spectrometry (RBS). Lectures given the workshop on Nuclear Data for Science and Technology: Material Analysis Trieste (2003).
5. H. R. Verma. Atomic and Nuclear Analytical Methods. Springer Berlin Heidelberg New York (2007). ISBN-10 3-540-30277-8.
6. K. C. Singh. Basic Physics. ISBN-978-81-203-3708-4.
7. The Rutherford scattering experiment. (2004).
8. www.physik.unibas.ch/Praktikum/VpII/PDF/Rutherford.pdf
9. Sven A. E. Johansson, John L. Campbell, Klas G. Malmqvist. Particle-Induced x-ray Emission Spectrometry (PIXE) (1995)
10. F. Corni, G. Ottaviani, M. Michelini, G. L. Michelutti, L. Santi, A. Stefanel. Rutherford Backscattering Spectrometry: A technique worth introducing into pedagogy. GIREP (1995).
11. S.A.E. Johansson and J.L. Campbell, and K.G. Malmqvist: Particle Induced x-ray Emission spectrometry (PIXE) (WILEY 1995)
12. Instrumentation for PIXE and RBS. IAEA, VIENNA (2000) www.pub.iaea.org/MTCD/publications/PDF/te_1190_prn.pdf.
13. B. D. Cameron, M. J. Rakovic, M. Mehrubeoglu. Measurement and calculation of the two-dimensional backscattering Mueller matrix of turbid medium. Optical Letters 23 (1998) 485-487.
14. Khalid Hossain. A Novel Process for Germanium Silicide Thin Film Synthesis. University of North Texas (2007).
15. http://mse.hanyang.ac.kr/SNE/.pdf.
16. G. Shmalz, V. Deutscher, U. Glatte and Ebenheit als physikalisches und physiologishes Problem. (1929) 1461-1467.
17. Apparatus for measuring surface irregularities. U.S. Patent 2,728,222.

18. Tunnel liner bolt tightening apparatus. UK Patent 2,009,409.
19. R. Young, J. Ward, F. Scire, The Topografiner: An Instrument for Measuring Surface Microtopography. Rev. Sci. Inst. 43 (1972) 999.
20. G. Binnig, H. Rohrer, Ch. Gerber, E. Weibel. Surface Studies by Scanning Tunneling Microscopy. Phys. Rev. Lett. 49 (1982) 57.
21. A. Escobedo Morales, E. S´anchez Mora, and U. Pal
22. Instituto de F´ısica, Benem´*erita* Universidad Aut´onoma de Puebla,Apartado Postal J-48, 72570, Puebla, Pue., M´exico
23. C, Richard Brundle,Charles A. Evans, Jr. Shaun Wilson. Encyclopedia Of Materials Characterization. Butterworth-Heinemann, a division of ReedPublishing, (1992).

CHAPTER 4

4 Result and Discussions

In this chapter, the obtained experimental data regarding the physical properties of SnSbS will be discussed. The discussion are mainly focused on four physical properties; (i) structural analysis ii) elemental analysis iii) optical analysis and iv) electrical analysis. The experimental data relating to these important physical properties were obtained by using XRD, SEM, RBS, Ellipsometry, PIXE and Hall measurement techniques. The results are discussed in detail to get a comprehensive analysis of the properties of target material in thin film form.

4.1 Structural Analysis:

The crystal structure, phase and composition of the deposited thin films of tin antimony sulfide by two source method thermal evaporation system were characterized by x-ray diffractometer with reference wavelength Cu Kα (λ=1.5405Å) radiation. The x-ray diffraction pattern for prepared thin films are shown in figure 4.1. The sharp peaks in this figure supports the polycrystalline behavior of these films. The preferential orientation of crystal planes in these thin films are (101), (104) corresponding to SnSbS and Sb respectively. There are also small peaks appeared in the XRD pattern of (003),(110),(021) corresponding to Sn and SbSn and shown in figure. 4.2. Qualitatively XRD patterns show that the compositions of SnSbS thin films are almost same as that of initial material. The diffraction angle 2θ slightly shifted towards higher angle with the addition of tin concentration in the Sb_2S_3. This is because of the fact that the thickness decreases when higher tin concentration in the film. The inter-planar distances d are calculated by using Bragg's formula which summarized in the Table 4.1. It is clear from the table that inter-planer distance "d" decreases as Tin concentration increases in Tin Antimony Sulfide films.

X-ray diffraction pattern peak angle wise are shown in figure 4.1 and elemental wise peaks are shown in figure 4.2. The pattern shows that tin doped antimony thin films are mainly orthorhombic structure(x-pert JCPD card # 00-035-1496) and also doping of sulfur does not change the crystal structure.

The particle size, interplanar distance and grain size were calculated by XRD using Scherrer's formula [1].

$$t = 0.9\,\lambda / \beta\cos\theta \quad \text{...} \quad (4.1)$$

Here 't' is grain size, wavelength 'λ' of x-ray ($\lambda = 0.154$ nm), 'θ' is Bragg's angle while 'β' is full width at half maxima .

Also formula for strain [2-5]. given in equation 4.2

$$\varepsilon = \beta\cos\theta \quad \text{..} \quad (4.2)$$

Where 'ε' is symbol used for strain. While we used the following Bragg's formula for the determination of Interplanar distance $d = \lambda / 2\sin\theta$.

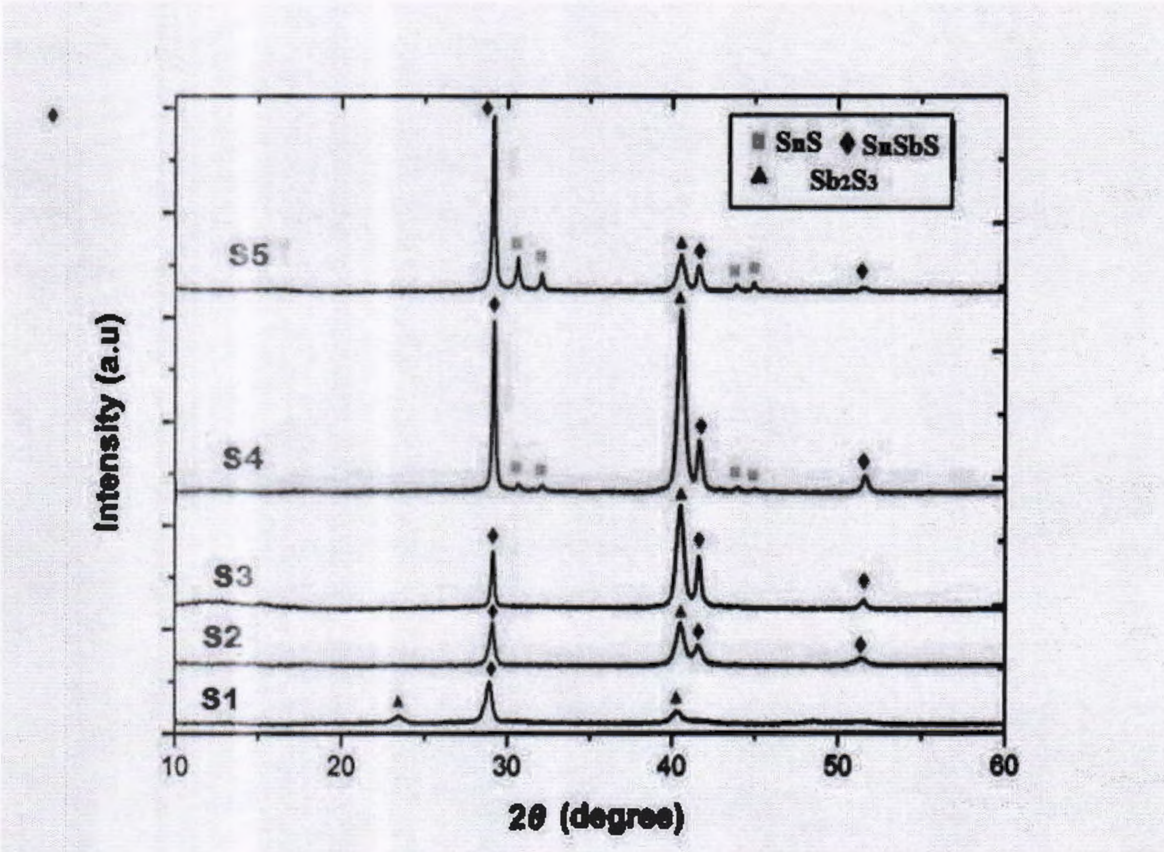

Figure 4. 1: XRD pattern for SnSbS thin films with varying contents of different elements

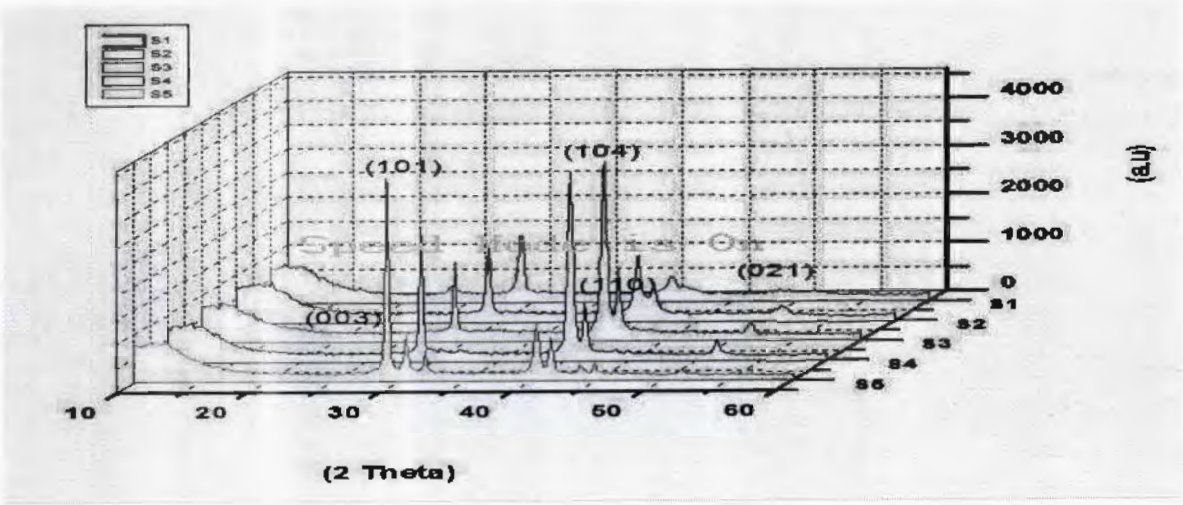

Figure 4. 2: 3-D XRD pattern of Tin antimony sulfide thin films

Table 4. 1: Structural data obtained from XRD measurement

Sample	2 theta (deg)	Hkl	d spacing Å	Thickness Å	Strain 10^{-4} lin^{-2}·m^{-4}	Lattice constant Å	Dislocation density 10^{14} lin·m^{-2}
S1	29.059	101	3.072	208	.394	4.344464	6.58
	40.486	104	2.228	179	.558	9.186279	7.7
S2	29.123	101	3.066	533	.259	4.335979	2.6
	40.531	104	2.225	239	.419	9.17391	5.7
S3	29.153	101	3.0633	417	.330	4.33216	3.26
	40.531	104	2.225	270	.371	9.17391	5.1
S4	29.199	101	3.060	464	.297	4.324665	2.98
	40.546	104	2.224	307	.325	9.169787	5.31
S5	29.192	101	3.059	523	.263	4.326079	4.03
	40.556	104	2.44	311	.418	10.06038	6.76

The deviation of dislocation density and strain with increasing Tin sulfide density indicates that minimum values of dislocation density and strain are observed at sample 2, while maximum is recorded at sample 5. The higher value of the dislocation density and strain obtained at sample 5 reveals the poor crystalline effect of Tin Antimony Sulfide films. While from S1 to S5 grain size increases and dislocation density decreases form S1 to S5. Small crystallites can fuse together to make larger crystallites, resulting in micro cracks and surface roughness. Annealing is well-known in reducing the stress of film as well as decreases the d-spacing.

4.2 Surface Morphology

4.2.1 SEM (Scanning Electron Microscope)

Scanning electron microscope (SEM) is best technique for surface morphology. The SEM images of the samples are shown in figure 4.3 to figure 4.6.

Figure 4. 3: SEM image of S1 (tin antimony sulfide)

Figure 4. 4: SEM images of S2 (tin antimony sulfide)

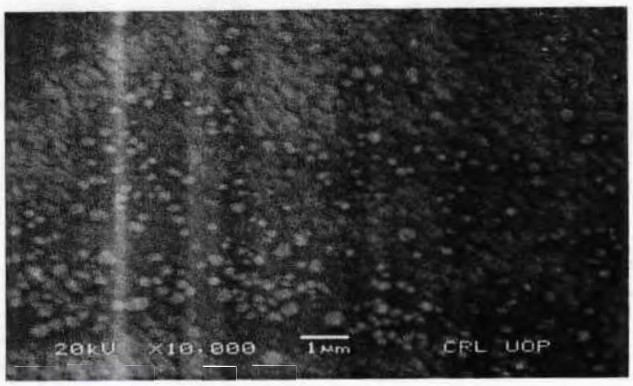

Figure 4. 5: SEM image S3(tin antimony sulfide)

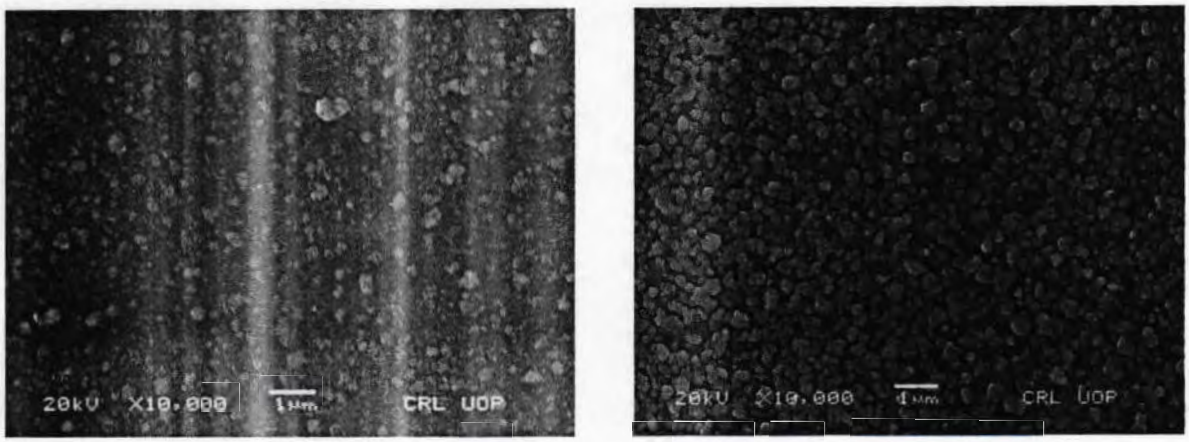

Figure 4. 6: SEM images of S4 & S5 (tin antimony sulfide)

The surface of samples look smooth and free from roughness but at micro level the surface samples shows little blisters on surface. Grain size and grain boundaries enhanced with increase in concentration of SnS. Small size grain merged together and also larger grains splits in to smaller grains and reoriented themselves which cause effect on whole structure. SEM images also indicates the decrease in roughness of layer by increasing concentration of SnS.

According to SEM images we calculated that the average grain size is almost 84.34 nm with beam energy 20 keV.

4.3 Elemental Analysis

4.3.1 RBS (Rutherford backscattering spectroscopy)

RBS technique used to determine the composition and thickness of the film like surface analysis technique. The basic principle is contained in the kinematics for binary collisions. A beam of known particles (ions) with mass M_1 is given the energy E_0 and directed onto the sample containing the particles M_2 that are to be investigated. RBS has been performed at data analysis lab National Centre for Physics (NCP). The parameters used for RBS was

- He^{++} ion beam
- Beam energy= 2.0 Mev
- Beam diameter= 2mm
- Beam current = 100 nAmp/cm^{-2}
- Back scattering angle =170°
- Detection with silicon detector

The gathered RBS spectra were then fitted by the code RUMP to locate the comparative concentrations of a mixture of elements in the films at Figure.4.7.

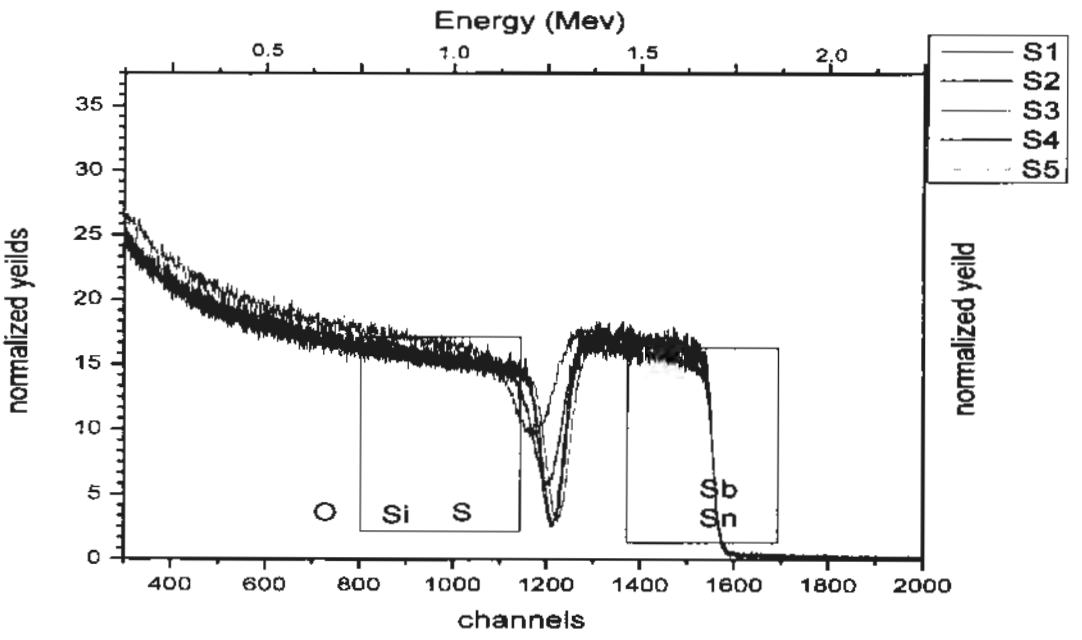

Figure 4. 7: Rutherford backscattering spectra of all samples

After annealing, as the RBS spectra turns into slightly broader and sharper so there could be a prospect of channeling. Annealing play an important part in altering the prominent change in elemental ratio with respect to stoichiometry within the layers has been observed as shown in figure 4.4. In RBS technique we conform the presence of tin, antimony and sulfur in all samples.

The thickness of film produce by on thin films is given in Table 4.2.

Table 4. 2: Thickness of thin film on glass substrate by RBS

Samples	Thickness By RBS (nm)
S1	238
S2	265
S3	268
S4	271
S5	290

4.4 Optical Analysis

The optical parameters like wavelength, refractive index, extinction coefficient, and band gap were calculated by ellipsometry technique by apparatus model name (J.A. Woolam M-200VI). The absorption coefficient of tin antimony sulfide was calculated by given mathematical relation,

$$a = 4\pi k/\lambda \quad \text{.....(4.4)}$$

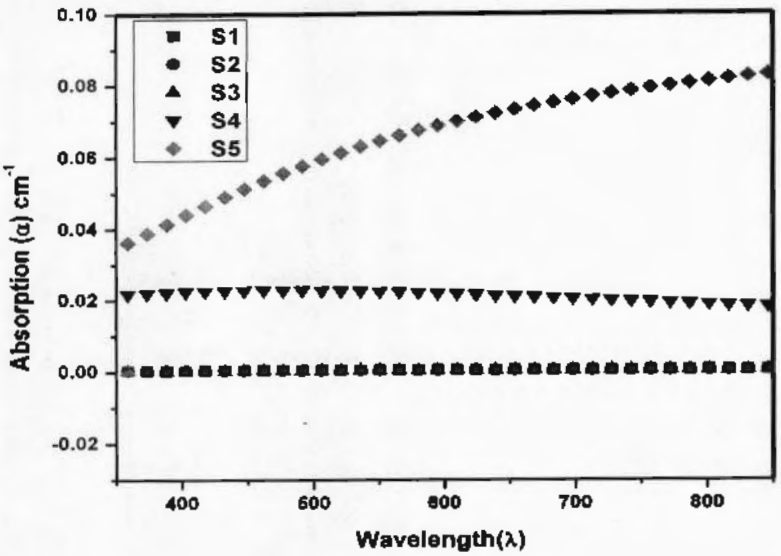

Figure 4. 8: Absorption coefficient of prepared thin films by Elipsometry

Where 'α'absorption and k is is coefficient of absorption. The graph of absorption coefficient and wavelength is shown in figure 4.6. Graph showing absorption is between the 0.001 to 0.9 cm^{-1} and can be easily sense a less absorption within the NIR region and visible region. The plot exposed that most of the light transmit in the visible light region (400 nm-700 nm) but somehow absorption happens for further higher wavelengths like 800 nm to 1100 nm.

Table 4. 3: Thickness of thin films by Ellipsometry

Samples	Thickness of films by Ellipsometry(nm)	%error
S1	348.39	.24
S2	347.12	.27
S3	352.47	.39
S4	236.14	.21
S5	335.43	.41

Band gap:

Band gap of the samples are calculated by ellipsometry which is shown in figure 4.9 to figure 4.13 which ranges 1.68 to 2.31 eV. And also thickness calculated by Ellipsometry given in Table 4.6. The formula used for the band gap measurements was given below in equation (4.5).

$$\alpha h\nu = A(h\nu - Eg)^{N/2} \quad \text{.....(4.5)}$$

Here A is a constant, hν = photon energy, Eg = optical band energy gap, and N depends on the nature of the transition (N = 1 for direct band gap and N =4 for indirect band gap transition).

While hν (eV) = 1240/nm.

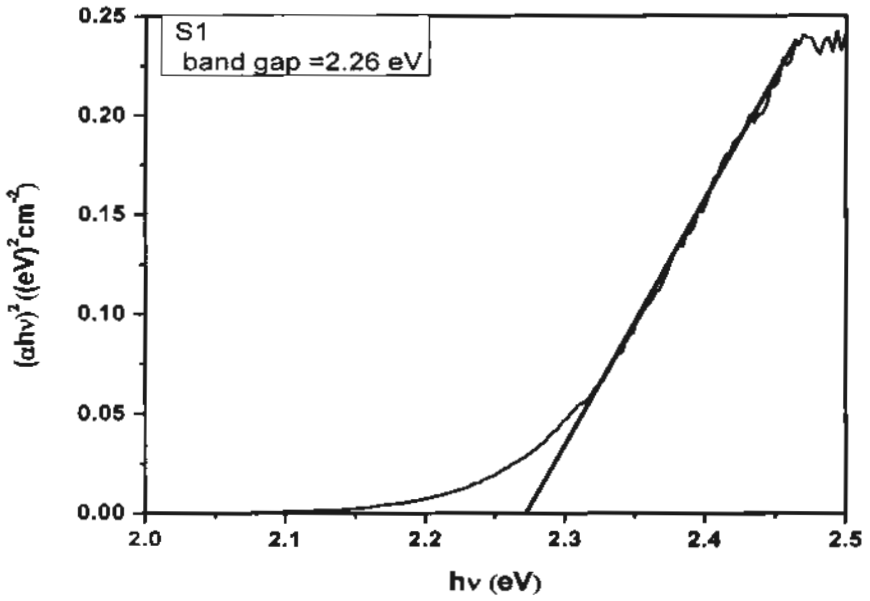

Figure 4. 9: Plotting band gap of prepared thin film for S1

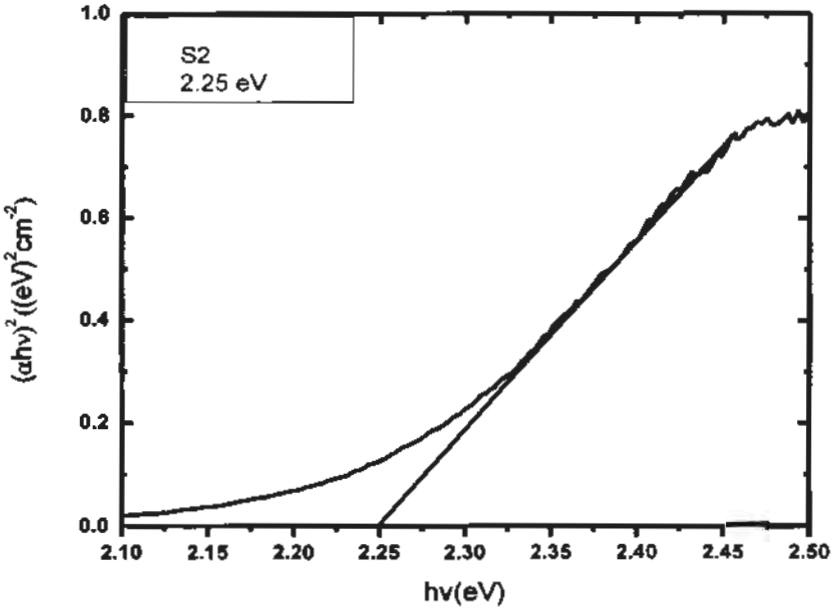

Figure 4. 10: Plotting band gap of prepared thin film for S2

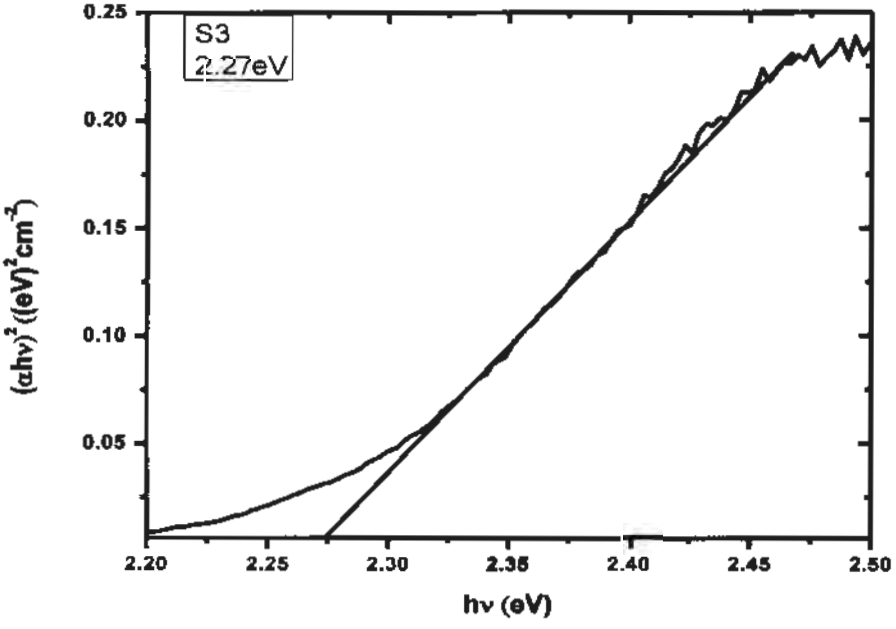

Figure 4. 11: Plotting band gap of prepared thin film for S3

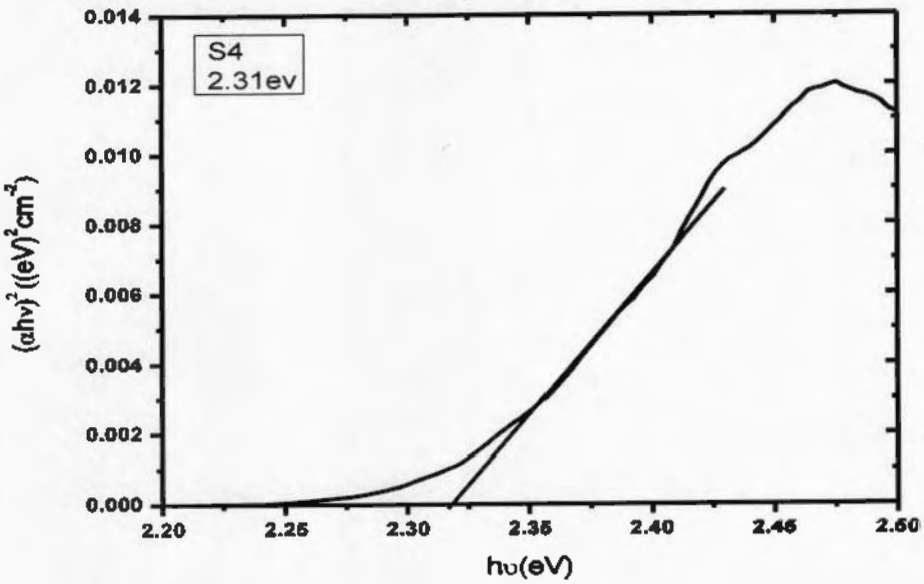

Figure 4. 12: Plotting band gap of prepared thin film for S4

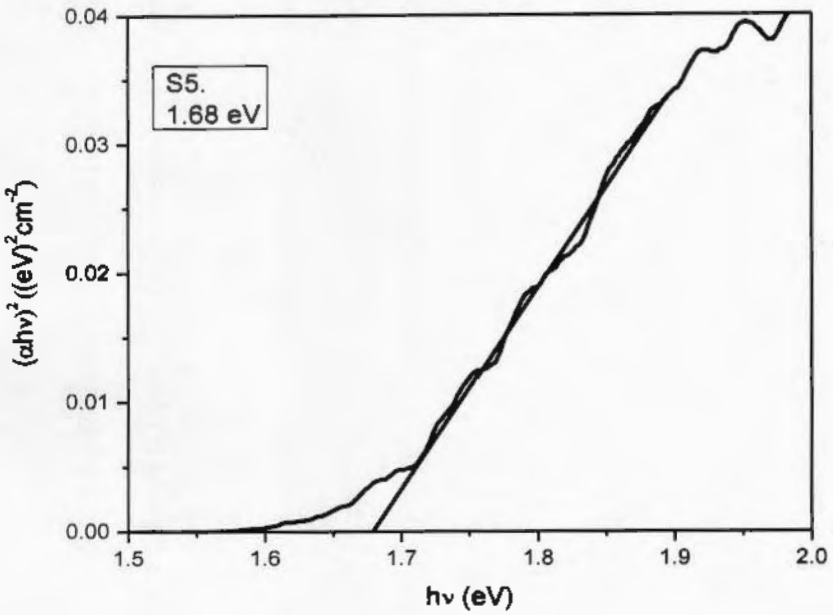

Figure 4. 13: Plotting band gap of prepared thin film for S5

4.4.1 Reflectance

The optical properties were analyzed from 350 nm to 850 nm wavelength by using ellipsometer at room temperature. Reflectance measurements were carried out by ellipsometry technique. The measurements were carried out on prepared thin films with varying tin sulfide concentrations. The relationship between the transmittance (T), absorption (A) and reflectance (R) has been given by equation (4.6).

$$T+R+A=1 \quad \text{.....} \quad (4.6)$$

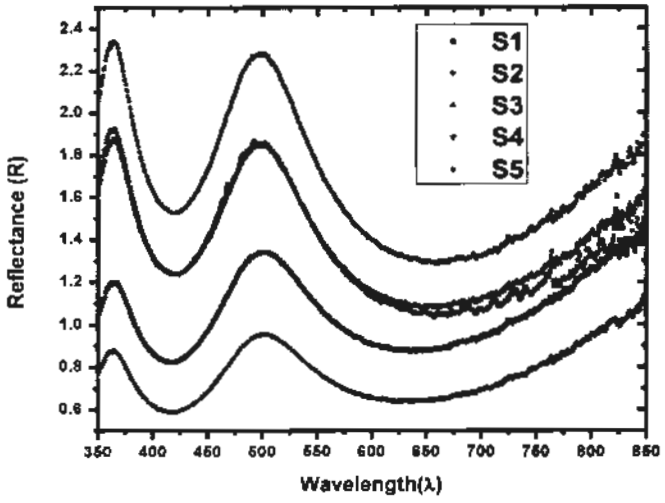

Figure 4. 14: Reflectance of tin antimony sulfide by ellipsometry

4.4.2 Extinction coefficient.

Extinction coefficient was measured by the equation given below equation (4.5).

$$K = \alpha\lambda/4\pi \quad \text{.....} \quad (4.5)$$

Where 'K' is the extinction coefficient, 'α' is the absorption coefficient and 'λ' is the wavelength Extinction coefficient 'K' was plotted against the wavelength and a marginal increase was observed in extinction coefficient with respect to increase in SnS concentration. The higher value recorded was for S5 concentration. However, value of '**K**' increased with increase in thickness of thin film and these results were matched with absorption coefficient results.

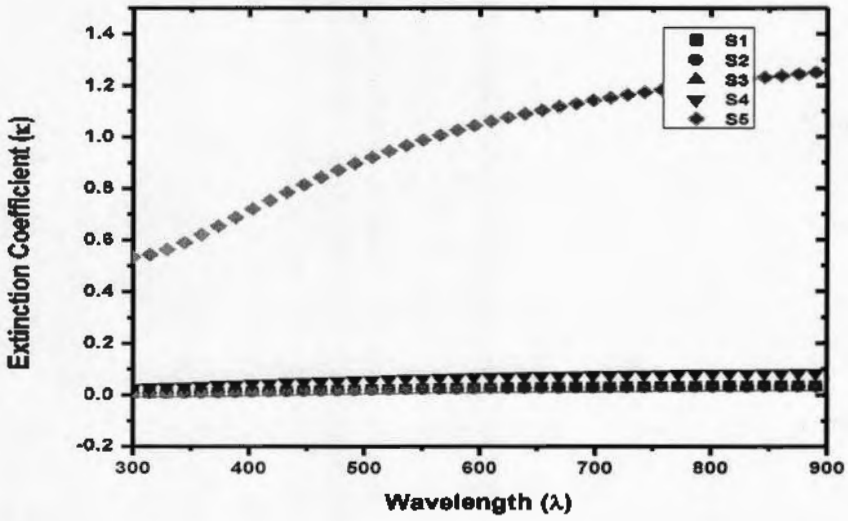

Figure 4. 15 : Extinction coefficient for $Sn_2Sb_2S_5$

4.4.3 Refractive index

The graph of refractive index n as a function of λ for Tin doped Sb_2S_3 films is plotted in the area of 300 nm to 950 nm and presented in figure 4.16. The plot demonstrate an unnatural dispersion in the range from 340 nm to 900 nm demonstrating many peaks. Finally we see that increasing contents of Sn increases in the refractive index of the thin film. The value of n is in between 0.9 to 1.4.

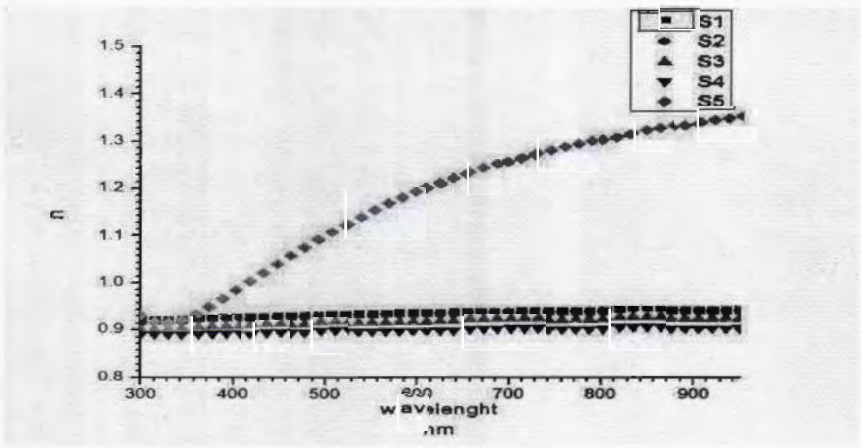

Figure 4. 16: Refractive index of Tin antimony sulfide

4.5 Electrical Analysis

Electrical analysis is done by hall measurement and two probe method and by finding the IV curve for sample and results are shown in table and graph. According to IV curve we see that the samples are highly conductive and by hall measurement we conformed that the samples are conductive having low resistive values, high carrier concentration along with high sheet carrier mobility.

The consequences of Tin density on thin films resistivity, mobility and carrier concentration were measured and the values are given in Table 4.4. Some of important parameters are that area of thin films were 1 cm^2 along with 0.55 Tesla constant magnetic field and 1 mA current were applied. Calculations shows that resistivity lowers its components with increasing Tin concentration. The resistivity decreases is mainly because of availability of large number of free charge carriers and enhanced structural properties as confirmed by XRD and SEM results.

The relation between mobility and resistivity shows that the mobility of carriers as well as the carrier concentration is enhanced with increasing Tin concentration. The carrier concentration increases with Tin component until it attains a maximum.

Table 4. 4 : Table for Hall Measurement

Sample	Sheet resistance (ohm/sq)	Resistivity (ohm.cm)	Conductivity (1/ohm-cm)	Sheet carrier concentration ($1/cm^2$)	Sheet carrier mobility (cm^2/Vs)
S1	3.21×10^{-1}	1.12×10^{-5}	8.94×10^{4}	-1.37×10^{19}	1.19×10^{1}
S2	1.86×10^{-1}	6.45×10^{-6}	1.55×10^{5}	-1.38×10^{19}	2.44×10^{0}
S3	1.03×10^{-1}	3.64×10^{-6}	2.75×10^{5}	-5.48×10^{18}	1.1×10^{1}
S4	9.93×10^{-2}	2.34×10^{-6}	4.27×10^{5}	-2.16×10^{19}	3.94×10^{0}
S5	1.68×10^{-1}	5.63×10^{-6}	1.78×10^{5}	-1.81×10^{19}	2.04×10^{1}

Where Rs: Sheet resistance; Rho: Resistivity; Con: Conductivity; Ns: Sheet carrier Concentration; μs: Sheet carrier Mobility. The mobility value for sample 1 is 11.9 $cm^2\ V^{-1}\ s^{-1}$ while for sample 5 is 20.4 $cm^2\ V^{-1}\ s^{-1}$. This increase in mobility is attributed to the availability of that free electron

charge carriers coming from the tin ions. In Sb_2S_3 sites tin ions are placed and decrease the grain potential barrier. The increase of mobility having lower value for samples S2 and S3 as compared to other samples, due to the increasing rate of scattering for charge carriers along with the formation of secondary levels as confirmed by the x-ray diffraction technique. In I-V measurement the evaluated electrical parameters support that Tin Antimony Sulfide thin films prepared by two source method demonstrate better electrical conductivity due to better crystalline quality also increase concentration of SnS. I-V plot are given in Figure 4.18.

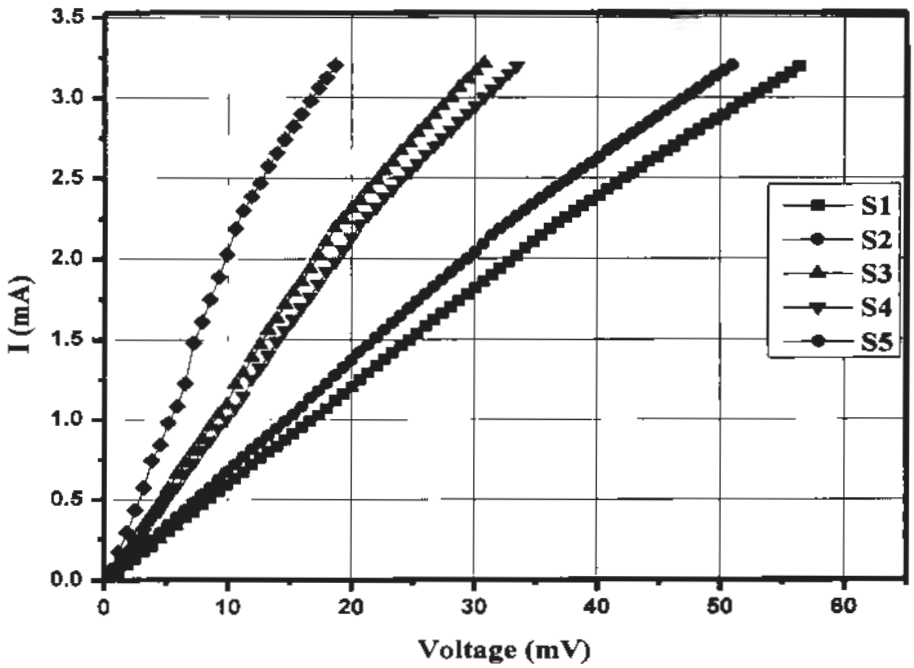

Figure 4. 17: Graph for I-V

As shown in plot that S5 is most conductive sample then other because of high concentration of tin. High value of resistance is recorded in S1 because of high concentration Sb_2S_3.

4.6 Conclusion:

Tin antimony sulfide was deposited on glass surface by two source evaporation vacuum thermal technique and then annealed in argon (Ar) gas environment at 150°C. The minimum crystallite size is calculated by x-ray diffraction pattern is 17.8 nm, while the average grain size measured from XRD calculations is 85.5 nm. Although the average grain size calculated from SEM images is 76.15 nm. We see the homogenous structure of thin films by SEM images and grains are uniformly distributed on thin films. The physical structure of Tin antimony sulfide on films thin films is polycrystalline nature mostly orthorhombic. The absorption coefficient of the thin film is very less make it good for multi-junctions solar cell. The material have direct band gap of 1.68 eV observed by ellipsometry and shows n-type conductivity. The refractive index is .9 to 1.4. All these structural and optical properties are very favorable for the multi-layer of solar cell.

4.7 References

1. Ali, N.; Iqbal, M.; Hussain, S.; Waris, M.; Munair, S., Optoelectronic Properties of Cadmium Sulfide Thin Films Deposited by Thermal Evaporation Technique. Key Engineering Materials **2012,** 510, 177-185.
2. M. Ashraf, S.M.J. Akhtar, A.F. Khan, Z. Ali and A.Qayyum, J. Alloys Compd. **509** (2011) 2414.
3. [15] E. Bacaksiz, S. Aksu, I. Polat, S. Y?lmaz and M. Altunbas,J. Alloys Compd. **487** (2009) 280.
4. [16] R. Kumar esan, M. Ichimura and E. Arai, Thin Solid Films **414** (2002) 25.
5. P.K. Kalita, B.K. Sarma and H.L. Das, Bull. Mater. Sci. **23** (2000) 313.